INVESTIGATION OF PHYSICAL PROPERTIES OF Gd DOPED Bi-2223 SUPERCONDUCTORS

by

MURAT ERDEM

THESIS SUBMITTED TO
THE GRADUATE SCHOOL OF NATURAL AND APPLIED SCIENCES
OF
THE ABANT İZZET BAYSAL UNIVERSITY
IN PARTIAL FULFILLMENT OF THE REQUIREMENTS FOR THE DEGREE OF
DOCTOR OF PHILOSOPHY
IN
THE DEPARTMENT OF PHYSICS

MARCH 2009

Approval of the Graduate School of Natural Sciences

Prof. Dr. Nihat Çelebi

Director

I certify that this thesis satisfies all the requirements as a thesis for the degree of Doctor of Philosophy.

Assoc. Prof. Dr. Ahmet Varilci

Head of Physics Department

This is to certify that we have read this thesis and that in our opinion it is fully adequate, in scope and quality as a thesis for the degree of Doctor of Philosophy.

Assoc. Prof. Dr. Cabir Terzioğlu

Co-Supervisor

Prof. Dr. İbrahim Belenli

Supervisor

Examining Committee Members

1. Prof. Dr. İbrahim Belenli .....

2. Prof. Dr. Ali Gencer .....

3. Assoc. Prof. Dr. Cabir Terzioğlu .....

4. Assoc. Prof. Dr. Ahmet Varilci .....

5. Asst. Prof. Dr. Erdal Bekiroğlu .....

ABSTRACT

INVESTIGATION OF PHYSICAL PROPERTIES OF

Gd DOPED Bi-2223 SUPERCONDUCTORS

Erdem, Murat

Ph.D., Department of Physics

Supervisor: Prof. Dr. İbrahim Belenli

Co-Supervisor: Assoc. Prof. Dr.Cabir Terzioğlu

March 2009, 103 pages

Many researchers have studied the effect of addition or substitution of different elements to high temperature superconductors. The aim in these studies is twofold; to understand the underlying mechanism of high temperature superconductivity and to enhance the mechanical and superconducting properties of the high temperature superconductors. The second purpose is especially important for the technological applications of the high temperature superconductors. Copper oxides (cuprates) are the most important group of high temperature superconductors. Among cuprates, the BSCCO system is widely studied and some technological applications are achieved. In this thesis, the effect of addition of Gd on the superconducting and mechanical properties of Bi-2223 phase is analyzed. The Gd ions are believed to substitute the

Ca ions of the BSCCO system. This is evidenced by the decrease of transition temperature (T_c) which is related to the charge carrier concentration and the decrease in the *c* parameter of the unit cell. The ionic radius of Gd is smaller than that of Ca so the decrease in the *c* parameter can be explained in terms of the difference in the radii. From the decrease of critical current density (J_c) values and SEM observations it is believed that the grain connectivity of the samples with increasing Gd content degraded. Weak link behaviour increased with the addition of Gd. The addition of Gd degraded the formation of the 2223 phase and hence as the Gd content increased, the volume fraction of 2223 phase decreased while that of 2212 increased. The high magnetic moment of Gd possibly affected the Cooper pairs in the superconducting phase. The spins of the pair may have been adversely affected by the magnetic moment of Gd which also resulted in the decrease of carrier concentration by pair-breaking mechanism. The results of this thesis showed that Gd addition degraded the superconducting and mechanical properties of the BSCCO system.

Keywords: Superconductivity, High Temperature Superconductors, Addition, Substitution, BSCCO system, mechanical properties.

ÖZET

Gd KATKILANMIŞ Bi-2223 SÜPERİLETKENLERİN
FİZİKSEL ÖZELLİKLERİNİN İNCELENMESİ

Erdem, Murat

Doktora, Fizik Bölümü

Tez Danışmanı: Prof. Dr. İbrahim Belenli

Yardımcı Tez Danışmanı: Doç.Dr.Cabir Terzioğlu

Mart 2009, 103 sayfa

Birçok araştırmacı farklı elementlerin yüksek sıcaklık süperiletkenlere katkılanmasının etkilerini araştırmaktadır. Bu araştırmaların iki amacı vardır; yüksek sıcaklık süperiletkenliğin temel mekanizmasını anlamak ve yüksek sıcaklık süperiletkenlerin mekanik ve süperiletkenlik özelliklerini geliştirmek. İkinci amaç yüksek sıcaklık süperiletkenlerin teknolojik uygulamaları açısından oldukça önemlidir. Yüksek sıcaklık süperiletkenler içerisinde bakır oksitler (kupratlar) en önemli gruptur. Bakır oksitler arasında BSCCO sistemi, yaygın olarak incelenmiş ve bazı teknolojik uygulamaları gerçekleştirilmiştir. Bu tezde, Bi-2223 fazına Gd katkılamanın süperiletkenlik ve mekanik özelliklerine etkisi incelenmiştir. Gd iyonlarının BSCCO sisteminde Ca iyonlarının yerine geçtiği düşünülmektedir. Bu

düşünce taşıyıcı yük yoğunluğuna bağlı olan geçiş sıcaklığındaki (T_c) ve birim hücrenin *c* parametresindeki azalma ile desteklenmektedir. Gd iyonlarının yarıçapı Ca iyonlarının yarıçapından küçüktür ve *c* parametresindeki azalma iyon yarıçaplarının farkı ile açıklanabilir. Kritik akım yoğunluğu (J_c) değerlerindeki azalma ve SEM görüntüleri, Gd içeriği arttıkça numunlerin tanecik bağlantılarının zayıfladığını göstermektedir. Gd katkısı arttıkça zayıf bağlantı özelliği artmaktadır. Gd katkısı 2223 fazının oluşumunu zayıflatmış ve sonuçta Gd katkısı arttıkça 2223 fazının oranı azalmış ve 2212 fazının oranı artmıştır. Gd elementinin yüksek manyetik momentinin süperiletken durumda Cooper çiftlerini etkilediği düşünülmektedir. Çiftlerin spinleri Gd elementinin manyetik momenti olumsuz etkileyerek çift-ayrışması etkisi de taşıyıcı yoğunluğunun azalmasına neden olabilir. Bu tez sonucunda BSCCO sistemine Gd katkılanmasının süperiletkenlik ve mekanik özelliklerini olumsuz etkilediği görülmüştür.

Anahtar Kelimeler: Süperiletkenlik, Yüksek Sıcaklık Süperiletkenler, Katkılama, yer değiştirme, BSCCO sistemi, mekanik özellikler.

To my family

ACKNOWLEDGEMENTS

At the very beginning, I must express that I owe a great deal to my supervisor Prof. Dr. İbrahim Belenli for his patience, support, guidance and supervision throughout this study. He gave me hope when I was in need.

I would express my gratitude to my Co-supervisor Assoc. Prof. Dr. Cabir Terzioğlu and Assoc. Prof. Dr. Ahmet Varilci for their valuable contribution during the discussions and their support.

I am also thankful to Hüseyin Aydın for his effort during the sample preparation and measurement.

TABLE OF CONTENTS

ABSTRACT…… iii
ÖZET…… v
ACKNOWLEDGEMENTS…… viii
TABLE OF CONTENTS……..…..…… ix

LIST OF TABLES ……..…xi

LIST OF FIGURES ……...xii

1 . INTRODUCTION ……1

1.1 SUPERCONDUCTIVITY ……..……2

1.2 HIGH T_c SUPERCONDUCTORS ……..…7

1.3 BSCCO SYSTEM ……..10

2. SUPERCONDUCTING PROPERTIES OF BSCCO……15

2.1 CRITICAL TEMPERATURE ……..…15
2.2 CRITICAL CURRENT …… 15
2.3 CRITICAL MAGNETIC FIELD …….. 16
2.4 CHEMISTRY OF THE BSCCO SYSTEM ……..…17

3. EFFECTS OF ADDITIONS INTO THE BSCCO SYSTEM ……18

3.1 ADDITIONS OF ALKALINE METALS ……..……..…19
3.2 Pb ADDITION …… 20
3.3 OXIDATION …… 21
3.4 ADDITION OF Hg …….. 21
3.5 ADDITION OF RARE-EARTH ELEMENTS …… 22

4.EXPERIMENTAL TECHNIQUES ……..…….34

4.1 SAMPLE PREPARATION ……..…….. 34
4.2 HEAT TREATMENT …… 35
4.2.1 CALCINATION …… 35
4.2.2 SINTERING ……35
4.3 CHARACTERIZATION OF THE SAMPLES …..…….. 39
4.3.1 R-T MEASUREMENTS …… 40
4.3.2 I-V MEASUREMENTS …… 41
4.3.3 XRD MEASUREMENTS ……..…… 42
4.3.4 SEM MEASUREMENTS ……..…. 45
4.3.5 MICROHARDNESS MEASUREMENTS……..….45

5. RESULTS AND DISCUSSION ……48

6. CONCLUSION ...……...…..…76

REFERENCES ……...….. 78

CURRICULUM VITAE ……..……..…..…….89

LIST OF TABLES

Table 1. Molecular weights of the chemicals used……34

Table 2. XRD reflection angles for BSCCO system……..43

Table 3. Results of XRD and resistivity measurements of the samples…….49

Table 4. The ionic radii of the cations……... 59

Table 5. The load dependent values of H_v, E, Y, and K_{IC} corresponding……65
to each sample calculated at 2.94 N.

Table 6. Best-fit results of experimental data according to Eq. (16)……..…69

Table 7. Best-fit results of experimental data according to Eq. (17)……..71

Table 8. Best-fit results of experimental data according to Eq. (18)……..73

LIST OF FIGURES

Figure 1. Physical properties of superconductors ……..…… 4

Figure 2. The interaction between the transport current density, magnetic flux and Lorentz force ……..…..……..5

Figure 3. The historical development of superconductivity……....9

Figure 4. The crystal structure of BSCCO system…… 12

Figure 5. Typical phase diagram with doping in cuprate superconductors ……. 23

Figure 6. Diagram of the sintering process……37

Figure 7. Preparation route of the samples……38

Figure 8. Drawing of connections in a transport measurement……40

Figure 9. X-Ray diffraction pattern for typical single phase samples of BSCCO….44

Figure 10. Resistivity vs temperature graph for Gd0,Gd2 and Gd4 samples……47

Figure 11. The graph of Equation 5..…….51

Figure 12. Transition temperature versus hole concentration……51

Figure 13. The variation of hole concentration with Gd content……....52

Figure 14. The variation of T_c offset with Gd content……..……...52

Figure 15. XRD results of the samples……...55

Figure 16. The graph of a parameter (2223) vs Gd content……57

Figure 17. The graph of c parameter (2223) vs Gd content……57

Figure 18. The graph of a parameter (2212) vs Gd content……58

Figure 19. The graph of c parameter (2212) vs Gd content……58

Figure 20. SEM micrographs of the Gd0, Gd2 and Gd4 samples……..62

Figure 21. Typical indentation for an applied load of 1.96 N for Gd4 sample…..….63

Figure 22. The variation of microhardness with load …..……..65

Figure 23. The variation of load dependent Vickers microhardness
of the samples as a function of Gd content……..…….67

Figure 24. Plots of diagonal length versus square root of applied
loads for the samples……..……..……68

Figure 25. Graph of the applied load against the square of the
diagonal length for the samples……..…….71

Figure 26. Plots of F/d versus d for the samples…….72

Figure 27. The variations of load independent Vickers microhardness
of the samples as a function of Gd content……..…….74

CHAPTER 1

INTRODUCTION

A common characteristic of copper-oxide high temperature superconductors (HTSC) is the presence of copper-oxygen planes. Superconductivity is confined to these copper-oxygen planes and T_c depends on the free charge carrier concentration in them. In most of the high temperature superconducting compounds which have been discovered so far, holes seem to be the dominant charge carriers. Apart from high T_c, ceramic superconductors have two other fundamental properties: a short Ginzburg-Landau coherence length ζ, and a large anisotropy. The small value of coherence length allows the achievement of high critical fields, H_{c2}, but thermal fluctuations in the mixed state in these materials play an important negative role. These fluctuations give rise to creep of the vortex lattice which causes dissipation [1].

Despite the attractive properties of all of the copper oxide superconductors, it is very difficult to obtain them in suitable form for various interesting applications, even if their superconducting properties are less sensitive to impurities than their metal counterparts, because of their ceramic character, small ζ and anisotropy. In these materials especially, one may expect that due to the small value of ζ, the effect of grain boundaries will be important. In order for them to reach their full potential the problems of processing ceramic superconductors must first be overcome.

Initial research on high-T_c ceramic superconductors in bulk ceramic form

revealed potential limitations for engineering applications. The brittle nature of the material and the high reactivity of the constituents make it difficult to synthesize this new family of superconducting compounds into usable form as wires, tapes, rods or composites.

Doping or substitution of HTSC materials with different elements is a widely used method for changing the superconducting and mechanical properties so that superconductors which can be used in technological applications can be achieved. Although BCS theory is successful in explaining the basic principles of superconductivity for type I superconductors, the mechanism of high temperature superconductivity is not completely understood. Doping or substitution of HTSC materials is also used for the examination of the basic principles of high temperature superconductivity by changing some parameters of the material and observing the effects associated with them.

This thesis is aimed at adding Gadolinium (Gd) to the high temperature superconductor $Bi_{1.8}Pb_{0.35}Sr_{1.9}Ca_{2.1}Cu_3Gd_xO_y$ (Bi-2223) and analyzing the changes in the superconducting and mechanical properties.

1.1 SUPERCONDUCTIVITY

Superconductivity was discovered in 1911 by Heike Kamerlingh Onnes [2], who was studying the resistance of solid mercury at cryogenic temperatures using the recently-discovered liquid helium as a refrigerant. At the temperature of 4.2 K, he observed that the resistance abruptly disappeared.

The next important step in understanding superconductivity occurred in 1933, when Meissner and Ochsenfeld [3] discovered that superconductors expelled applied magnetic fields, a phenomenon which is known as the Meissner effect.

There are two types of superconductors: type I and type II. For type I superconductors, the superconductivity can be destroyed by applying external magnetic field higher than the critical value B_c. If the applied magnetic field is less than B_c, then it is entirely expelled according to the Meissner effect. The exclusion of external magnetic field is provided by the generation of shielding currents set up in the surface of the superconductor which create a magnetic flux equal and opposite to the external flux.

Superconductivity can also be destroyed by passage of a current greater than the critical value I_c of a superconductor. Type I superconductors are generally pure metals. In these superconductors critical magnetic flux and critical currents are low so their practical use is limited.

For type II superconductors, magnetic flux can penetrate into the superconductor in the form of localized flux lines. Each of these fluxes carry a single quantum of magnetic flux

$$\Phi_o = ch/2e = 2.0678 \times 10^{-7} \text{ gauss.cm}^2 = 2.0678 \times 10^{-15} \text{ tesla.m}^2$$

and the material remains superconducting up to a value of magnetic flux (B_{c2}). At B_{c1} the flux starts to penetrate the material and at B_{c2} the material becomes normal. These basic properties of superconductors are shown in Fig. 1. The external magnetic field does not fall to zero at the surface but decays exponentially inside the superconductor. The distance of flux penetration is called penetration depth (λ).

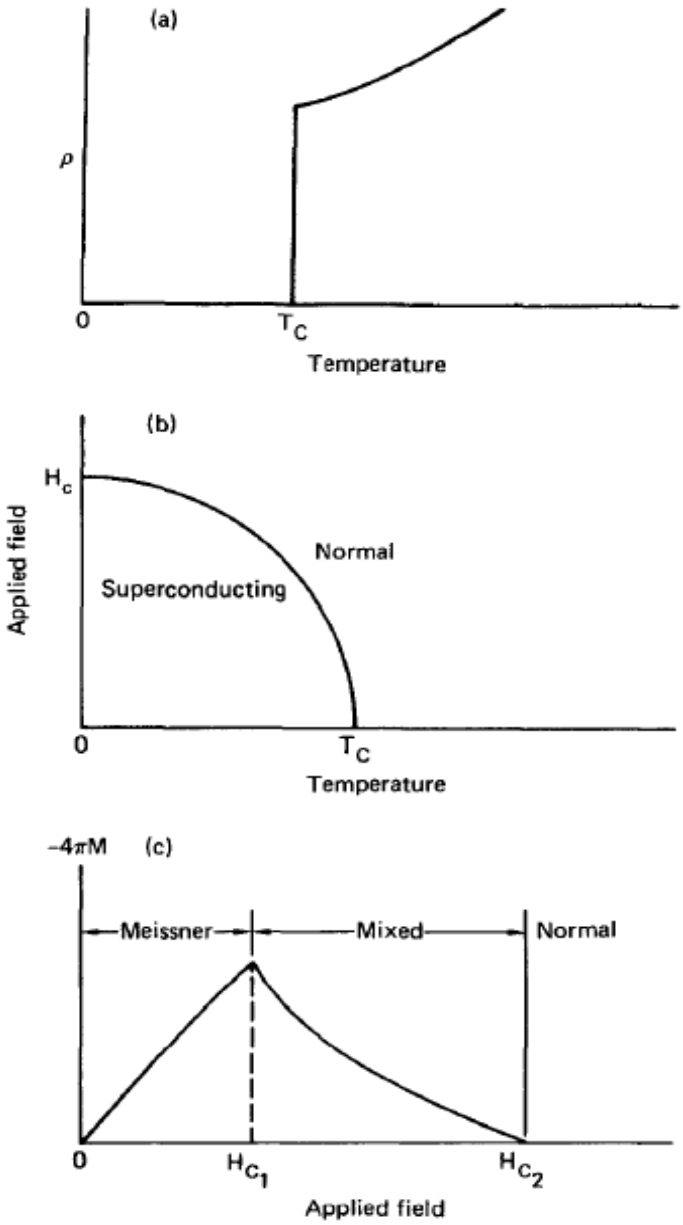

Figure 1. Physical properties of superconductors. (a) resistivity disappears below T_c. (b) Type I superconductors exhibit perfect diamagnetism up to a critical field H_c. (c) Type II superconductors exhibit perfect diamagnetism up to a field H_{c1}, enter a mixed state between H_{c1} and H_{c2}, then exhibit normal metal behavior above H_{c2}.

When a type II superconductor is in a magnetic induction greater than B_{c1}, where a flux line penetrates the surface it consists of a normal core surrounded by circulating supercurrent in a cylinder with radius of the order of the penetration depth. At this stage, if a current of density J_c is passed through the superconductor, flux lines experience a Lorentz force **F = JxB**. Under the action of this force, the flux lines will try to move and if they do so will generate an induced emf and hence an electrical resistance. This phenomenon is known as flux flow which is shown in Fig. 2. If this happens, the passage of current will be no longer lossless. The motion of flux lines can be prevented if they are pinned, for example if they are able to interact with microstructural defects such as dislocations, grain boundaries and precipitates of a second phase in the superconductor.

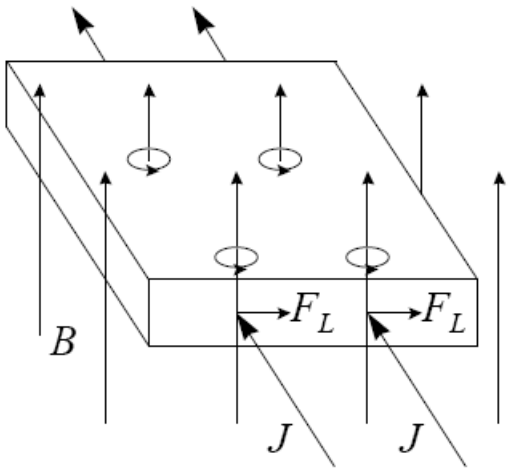

Figure 2. The interaction between the transport current density J, magnetic flux B, and Lorentz force F_L in a Type II superconductor in the mixed state. Supercurrent vortices ring the fluxoids. The fluxoids remain stationary as long as F_L is less than the flux pinning force Fp.

To explain the superconductivity in low T_c materials, BCS theory was developed by Bardeen, Cooper and Schriffer [4] in 1957. It explains most of the observations in conventional metallic superconductors, such as the change in T_c with isotope effect and predicts the existence of a critical current density (J_c).

BCS theory shows how the electron-phonon interaction can result in an indirect attractive force between electrons. Electrons and ions that form the lattice are oppositely charged. Any electron in its motion through the lattice polarizes the lattice along its path and the polarization remains for the time required for the phonons making up the ion displacements to disperse. This time for dispersion is sufficiently long to allow another electron to experience the local polarization caused by the first electron. Its potential energy is thereby reduced, so it can be considered that through the intermediacy of the phonons the electrons can have an effective attraction between them at a distance. The average maximum distance at which the phonon coupled attraction can occur is called the coherence length (ζ). This attraction of the two electrons of a pair (called a Cooper pair), which lowers the energy of the pair relative to the mean energy (Fermi energy) of the unpaired electrons, is greatest when they have opposite spins and equal and opposite wave vectors. The exchange of a virtual phonon pairs electrons with opposite wave vectors, so that the pair cannot be scattered without breaking up and increasing the energy of the system. Hence there is no resistance to the flow of electrons.

According to the BCS theory of superconductivity the transition temperature is given as:

$$k_B T_c = 1.14\hbar\omega_D \exp\left[\frac{-1}{N(0).V}\right] \quad (1)$$

So it is seen that transition temperature depends strongly on the density of available states i.e. hole concentration.

The decreasing of the energy of the system on electron pairing results in an energy gap of magnitude 2Δ, in the band structure of a superconductor at the Fermi surface. The Cooper pairs lie in a condensed state at the Fermi energy and the excited quasi-particle states lie at an energy Δ above the Fermi energy. BCS theory predicts a value of

$$2\Delta_o / kT_c = 3.52 \quad \text{at 0 K}$$

which is fairly well obeyed in conventional metallic superconductors.

1.2 HIGH T_c SUPERCONDUCTORS

The BCS theory is quite successful at explaining the properties of most superconductors. But the discovery in 1986 of a new class of materials that superconduct at high temperatures remains a challenge to theorists, and there is still no unambiguous theoretical explanation for this phenomenon.

Until 1986, physicists had believed that BCS theory forbade superconductivity at temperatures above about 30 K. In that year, Bednorz and Müller [5] discovered superconductivity in a lanthanum-based cuprate perovskite material, which had a transition temperature of 35 K. It was shortly found

by Wu et al. [6] that replacing the lanthanum with yttrium, i.e. making YBCO, raised the critical temperature to 92 K, which was important because liquid nitrogen could then be used as a refrigerant. Superconductivity at liquid nitrogen temperature (77K) was at last a reality. This discovery accelerated the research efforts to discover new compounds with higher T_c. In Fig. 3 the historical development of superconductivity is shown.

A common feature of copper-oxide based superconductors is their perovskite layered crystal structure consisting of one or more two-dimensional CuO_2 planes (in one unit cell) separated by varying thicknesses of non-superconducting planes containing other cations and oxygen such as SrO, LaO, CuO, PbO, BaO, BiO, and TIO, or planes containing just cations such as Y or Ca. It appears also that both CuO and CuO_2 planes are present. A feature common to these perovskites is their variability in oxygen content and the sensitivity of the properties of interest to the amount of intercalated oxygen.

Some of the properties of the new high T_c oxides are quite different from those of the conventional low T_c superconducting metals and alloys. Most prominent is the low critical current density of polycrystalline samples, one of the outstanding problems that needs to be solved for large scale applications. There is experimental evidence that grain boundaries, even if free of second phase material, act as weak coupling junctions between grains rather than as pinning centers. On the other hand, very high critical current densities have been achieved in high quality oriented films and single crystals. Their unconventional properties are results of their short coherence length, rather than to a radically different type of superconductivity.

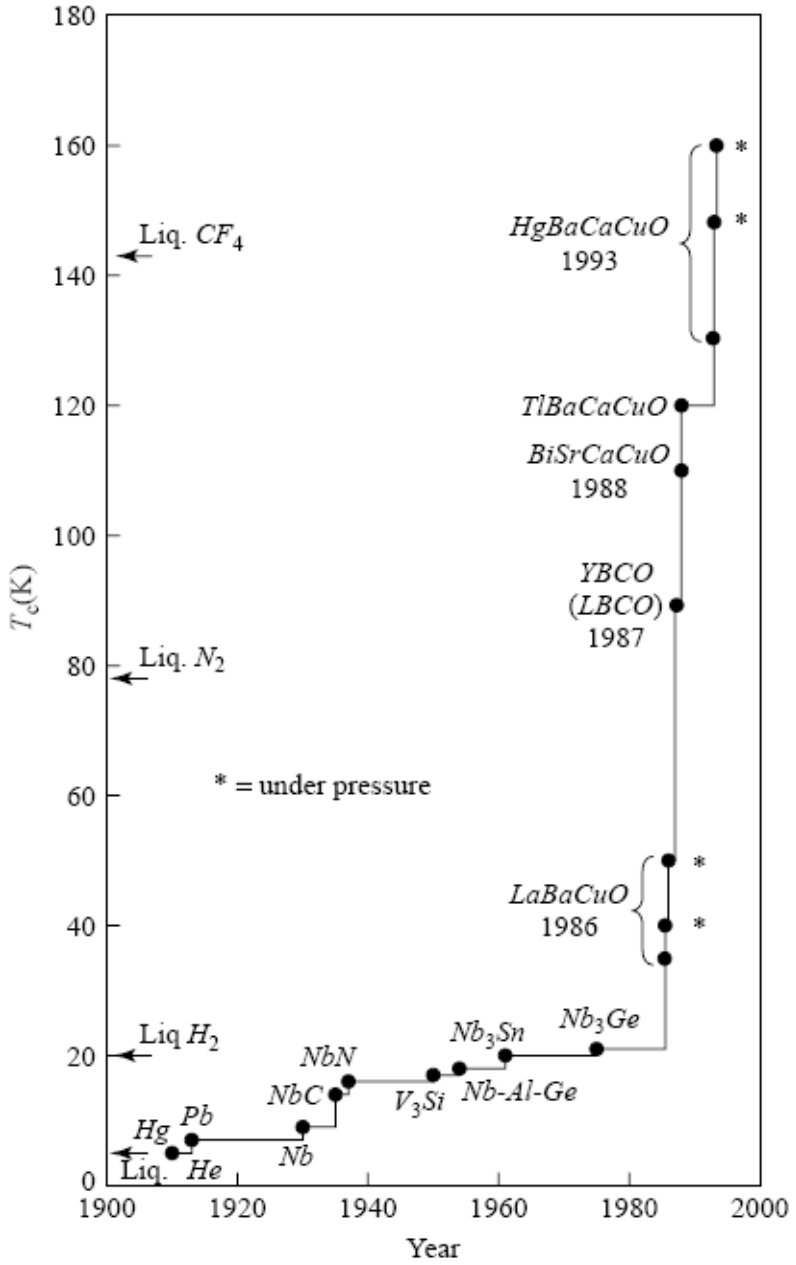

Figure 3. The historical development of superconductivity

Due to this short coherence length, the superconducting order parameter is very sensitive to defects on the atomic scale. The superconducting properties were found to be highly anisotropic, with the superconducting electrons basically confined to the Cu-O planes which lie on the basal plane because of the extremely short coherence length along the *c*-axis.

High-T_c materials, which are doped oxides, are made by heating a mixture of appropriate amounts of metal oxides in powder form to temperatures in the range 800–950 ^{o}C. Materials that contain some percentage of superconductor are then obtained. But making materials of good quality, whether polycrystalline or single crystals is quite a different and highly non-trivial matter. Great attention must be paid to every detail of composition, temperature, pressure and atmosphere to obtain high quality materials. Repeatedly grinding, compressing and sintering is usually necessary. The resulting bulk material is then a fine-grained ceramic, brittle, and with high density of defects and grain boundaries.

1.3 BSCCO SYSTEM

In 1988, H.Maeda et al. [7] discovered a new high-T_c oxide superconductor of the Bi-Sr-Ca-Cu-O (BSCCO) system. The oxide $BiSrCaCu_2O_x$ has T_c of about 105 K, higher than that of $YBa_2Cu_3O_7$ by more than 10 K. In this oxide, the coexistence of Sr and Ca is necessary to obtain high T_c. Since then great amount of work has been done on this system to improve the superconducting properties, to understand the underlying physics and to make technical applications possible.

There are three different phases of the BSCCO system which are called 2201,

2212 and 2223 according to their chemical stoichiometric compositions. These phases have critical transition temperatures of 20 K, 85 K, and 110 K respectively. These phases can be formulated as: $Bi_2Sr_2Ca_{n-1}Cu_nO_x$ where n=1,2,3. These phases differ by the number of Cu-O layers in their crystal structure as shown in Fig. 4. The crystal parameters of the three phases are :

a=b=5.4 Å , c=24.4 Å for 2201 phase

a=b=5.4 Å , c=30.7 Å for 2212 phase

a=b=5.4 Å , c=37.1 Å for 2223 phase

The number of copper-oxide planes is closely related to T_c, it increases with the number of Cu-O layers. The 2201 phase is not much studied in the literature due to its low T_c value. The 2212 phase is known as the low T_c phase. The 2223 phase is known as the high T_c phase. The weak link grain boundaries lead to highly magnetic field-dependent critical current, decreasing considerably in a small magnetic field. The critical current density, J_c does not depend only on the field strength but also on the field direction due to anisotropy. Flux creep is particularly a problem in BSCCO, and so much effort has concentrated on improving and controlling microstructure and grain orientation.

Under normal preparatory conditions, the 2212 type appears to be the most stable and is often the most dominant in presence even when the starting composition was aiming for 2223. The 2223 phase can be gradually stabilized with annealing just below the melting point. With 15% of Bi replaced by Pb, the 2223 type can be prepared in pure form.

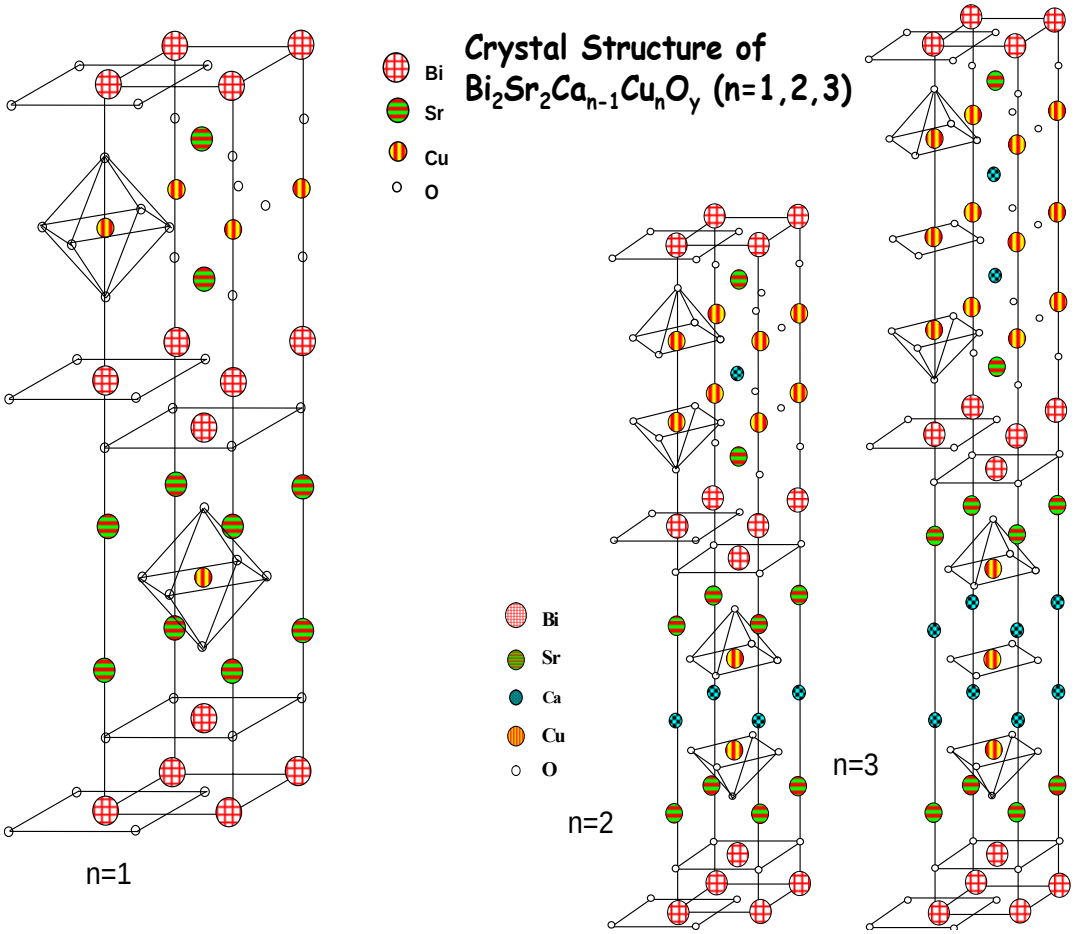

Figure 4. The crystal structure of BSCCO system

By T_c measurement alone, the individual member of the BSCCO family can be distinguished and studied separately. Therefore the BSCCO group provides the best opportunity to study the individual structure-related properties in the normal as well as superconducting states [8].

Superconductivity in the Bi-based system is studied by a large number of researchers, but to obtain good superconducting poperties a careful processing is necessary. One advantage of the Bi-based system is that it does not contain poisonous elements unlike the Tl based superconductors.

The simplest copper oxide perovskites are insulators. In order to become superconducting, they should be doped by charge carriers. There are two ways to increase the number of charge carriers in cuprates chemically: (i) to substitute metallic atoms in the intermediate planes by higher-valence atoms and/or (ii) to change the number of oxygen atoms. Doping increases or decreases the number electrons or holes at the Fermi level. The concentration of charge carriers in HTSC is low (5×10^{21}), in comparison with conventional superconductors (5×10^{22}–10^{23}). However, due to the large coherence length in conventional superconductors, only a 10^{-4} part of the electrons, located near the Fermi surface, participate in coupling. At the same time, in cuprates, about 10% of all conduction electrons (holes) form the Cooper pairs.

In most of hole-doped cuprates, the $T_c(p)$ dependence has the bell-like shape and can be approximated as [9]

$$T_c/T_c^{max} = 1 - 82.6\,(p - 0.16)^2 \qquad (2)$$

where T_c^{max} is the maximum critical temperature for a given compound.

Superconductivity occurs within the limits, $0.05 \leq p \leq 0.27$, which vary slightly in various cuprates. Thus, the different doping regions of the superconducting phase may be chosen such as the underdoped, optimally doped and overdoped regions. The insulating phase at $p < 0.05$ is called the undoped region, but above 0.27, cuprates become metallic.

CHAPTER 2

SUPERCONDUCTING PROPERTIES OF Bi-BASED SYSTEM

2.1 CRITICAL TEMPERATURE

The critical temperature T_c of a superconductor is the temperature at which the transition between superconducting to normal states occurs. The critical temperatures of the high T_c ceramic superconductors are much higher than those of the conventional superconductors (hence the name high T_c). But generally the transition width is broader in high T_c supercondutors when compared to the conventional superconductors. To define T_c , T_c onset and T_c offset points must be determined. T_c onset is the temperature at which the resistive behaviour of the sample changes from straight line metallic or slightly curved to a significantly curved one. T_c offset is the temperature at which zero resistivity is reached. To determine the above values, the derivative of resistivity versus temperature graph is drawn. The maximum value of the derivative function is the T_c which is the midpoint of the T_c onset and T_c offset values. The point where the function starts to increase (while temperature is decreasing) is the T_c onset value and the T_c offset value is the point at which the function stops decreasing.

2.2 CRITICAL CURRENT

The critical current density (J_c) is usually the most important property of a superconductor as far as practical applications are concerned. Many researchers conducted studies to observe higher values for J_c. J_c is especially important for

magnetic field production by superconductors and power line transmissions. The critical current density of superconductors decrease drastically under magnetic field due to flux flow. Flux pinning centers are needed to prevent flux flow. High T_c oxides are highly anisotropic so in bulk form their current density is rather low for polycrystalline structures. For single crystals and thin films much higher J_c values are obtained. The critical current density of high T_c oxide superconductors is microstructure dependent.

There are serious limitations for current carrying capacity of high T_c oxide superconductors. Due to random grain growth during annealing or grain misalingment gives rise to porosity. Also grain boundaries acting as weak links degrade current density. Especially misalignment of grains with respect to each other degrades J_c drastically with increasing angle of misalingment. Impurities decrease the superconducting volume fraction and cause irregularities in the cross-section of the superconductor. The critical current densities are not very high for applications. It is very much dependent on the microstructure. Especially bulk superconductors have pores in the material due to random growth of the grains during the heat treatment. Impurities in the material decrease the density (volume fraction) of the superconducting phases and hence decrease the critical current density.

2.3 CRITICAL MAGNETIC FIELD

High T_c superconductors have very high H_{c2} values. They can be better suited for magnetic field production compared to conventional superconductors. This property must be handled in conjunction with the need to obtain high enough critical current densities. Flux pinning is important for the achievement of high J_c under high magnetic fields.

Before HTSC can be applied to technology, the mechanical problems associated with them must also be solved. These HTSC are very brittle. During the production processes they will be prone to mechanical deformations and stresses like bending. Mechanical effects degrade the superconducting properties of HTSC materials. Cracks can easily be formed within the superconductor.

2.4 CHEMISTRY OF THE Bi-BASED SYSTEM

In our study, we produced samples of the 2223 phase. The formation of the 2223 phase in the pure BSCCO specimen is an extremely slow process [10]. The 2212 phase is more stable than the 2223 phase so it is easier to obtain the 2212 phase. The 2223 phase is formed from the 2212 phase. When producing samples it is likely to have multiphases containing both the high and the low phases. It is important to have a phase pure sample in order to see the superconducting and physical properties of the phases seperately. At the beginning of annealing process, the 2201 phase forms first from amorphous precursors and it evolves to the 2212 phase by solid state reactions. Later the 2223 phase forms from the 2212 phase [10]. A partial melting advocates fast diffusion paths for the formation of the 2223 phase. For the production of the 2223 phase, non-stoichiometric compositions where one or more elements are slightly different than their theoretical fraction are used. The preparation conditions such as annealing temperature, anneling time and ambient are also important for the high T_c phase formation [11].

CHAPTER 3

EFFECT OF ADDITIONS INTO THE BSCCO SYSTEM

As stated above, the high-T_c (2223) phase, with the highest T_c among the family is very difficult to prepare in a single phase. However, partial substitution of Pb for Bi has already been confirmed to aid the growth of the 2223 phase. It was also found that the properties of Bi,Pb–Sr–Ca–Cu–O materials can be changed by the substitution or addition of the elements having different ionic radii and valency. The superconducting properties are either enhanced or destroyed, depending on the characteristics of the dopant in the crystal structure.

It is clear that whenever the substitution decreases the number of charge carriers (holes for BSCCO system), the superconductivity is suppressed. Weak coupling between BiO–BiO layers in the BSCCO system enables the substitution of the different oxides for Bi^{3+} site. Some of the results have demonstrated that there is no significant increase in the T_c. But, important changes occur in the carrier concentration due to the different cation doping levels. Therefore, the electrical property of the system varies.

T_c of superconducting copper-oxide based compounds depends on the density of mobile holes in the CuO_2 planes and thus on the average Cu valancy. The replacement of Ca^{2+} ions by Gd^{3+} ions leads to a decrease of the formal Cu valancy, whereas, the substitution of Pb^{2+} in Bi^{3+} site increases Cu valancy. As a result, T_c decreases with increasing Gd content, whereas it increases with a small amount of Pb

substitution. So superconducting properties are strongly affected by changes in the hole concentration induced by the amount of doping.

Many elements have been doped into the BSCCO system. The doping is done to optimize the hole concentration, to introduce pinning centers and to enhance the formation of the 2223 phase. So high values for T_c and J_c are expected to be produced. Understanding the mechanism of the change in the normal state properties as well as the superconducting properties with varying dopants and dopant ratios are needed to understand the physics behind superconductivity better.

3.1 ADDITIONS OF ALKALINE METALS

There have been several studies on the effects of alkaline metal (Li, Na, K, Rb and Cs) substitution or addition on the superconductivity in the Bi-based superconductors since their ionic radii overlap those of Bi, Pb, Sr, Ca and Cu. Furthermore, alkaline metals have a +1 valence state, so that their addition is attractive from the point of changing carrier concentrations [12]. Kawai et al. [13] studied the effects of alkaline metal substitution in $Bi_2Sr_2CaCu_2O_x$. They found that alkaline metals drastically decrease the formation temperature of the 2212 phase. T_c was increased by Li and Na doping, but was decreased by K and Rb doping. Li doping resulted in the highest onset of superconductivity (T_c= 98 K) and the largest superconducting volume fraction. Although, there has been considerable work on alkaline metal substitution or addition in the Bi-based system, it has mainly focused on the 2212 phase. Petrasko et al. [14] studied the influence of alkaline metal dopants on the structure and superconducting properties of the Bi-2223 system. Doping with K, Rb and Cs to level of 30 mole % leads to an increase in T_c, critical current density J_c and decrease

in the normal state resistance.

The influence of Cs doping and heat treatments on the phase formation, microstructure development and normal, superconducting state properties of Bi,Pb–Sr–Ca–Cu–O superconductors was systematically investigated by Zhigadlo et al. [15]. Addition of Cs to $Bi_{1.7}Pb_{0.3}Sr_2Ca_2Cu_3O_y$ was found to be effective in forming the high-T_c 2223 phase. The superconducting properties were enhanced with Cs doping.

3.2 Pb ADDITION

The addition of Pb greatly enhances the formation of the Bi(2223) phase resulting in almost single-phase samples, since Pb enlarges the Bi(2223) formation domain. By the conventional route starting from oxides and carbonates the low-T_c phase or Bi(2212) forms first and is then transformed into Bi(2223) [16].

Whereas the Bi(2201) and Bi(2212) compounds can readily be synthesized either from the melt or using solid state reaction, the Bi(2223) phase is quite difficult to produce with acceptable purity. However, the partial replacement of Bi by Pb in the crystal lattice of this latter phase was reported to greatly enhance the phase formation kinetics and the quality of the Bi(2223) phase samples [17,18]

Partial substitution of Pb for Bi in the Bi-Sr-Ca-Cu-O system has been found to sharply increase the volume fraction of the high-T_c phase when both the starting material and the heating process are appropriate. M. Takano et al. [19] conclude that the addition of Pb combined with an appropriate fabrication process not only creates a reaction path more advantageous to the formation and growth of the high-T_c phase but also increases the thermodynamical stability of this phase.

Ibrahim et al. studied the effect of Pb addition on T_c and microhardness and concluded that the addition of (0.3Pb) resulted in an increase in T_{co} from 93 to 113 K and a 2.85-fold increase in the microhardness. This behavior is ascribed to the presence of large amount of the high-T_c phase (2223) [20].

Addition of Pb into the BSCCO system improves the mobility of the ions resulting in a faster growth of the 2223 phase.

3.3 OXIDATION

The superconducting properties of both 2212 and 2223 phases are also dependent on the oxygen content. 2223 phase shows lower T_c when deprived of oxygen [11]. The excess oxygen is considered to be responsible for superconductivity. Oxidation of the samples is done by annealing under oxygen rich or low atmospheres. Deoxidization is done by annealing under vacuum or under low partial pressures of oxygen or under atmospheres of other gases.

3.4 ADDITION OF Hg

Shelke et al. studied the effect of Hg addition on synthesis of BSCCO with both types of starting compositions 2212 and 2223, the finally obtained phase was Bi-2212. Neither any mercury-related phase was formed nor mercury was incorporated in the system. Thus, the role of Hg was like a catalyst. The maximum T_{c0} obtained is 92 K is within the range of that obtained by proper tuning of hole concentration. At the same time, T_c depression with 2212-type starting composition is observed. Such a

variation of T_c has been attributed to the tuning of optimal charge carrier concentration. Also, an improved grain diffusion has been observed in the highest T_c samples [21].

3.5 ADDITION OF RARE- EARTH ELEMENTS

The well-established phase diagram of the CuO_2-based superconductors is that the systems are insulating in the low-carrier-concentration region and superconducting in the intermediate range, whereas in the heavily doped region they are normal metals [22,23,24,25,26]. The carrier concentration in the high-T_c systems may be varied by varying the dopant and oxygen content. T_c increases with the increase of the carrier concentration, passes through a maximum, and then decreases and becomes zero beyond a critical concentration. The concentration at which maximum T_c is observed varies from system to system. The maximum value of T_c for $(Bi_{1-x}Pb_x)_2Sr_2Ca_2Cu_3O_{10+y}$ system is observed for x=0.20 [27,28]. The T_c versus n_H (hole concentration) plot follows a universal domeshaped curve as shown in Fig. 5. For the 2212 system, superconductivity appears above a carrier concentration of 0.07 holes/Cu. T_c increases with the increase of the carrier concentration, passes through a maximum at about $n_H = 3 \times 10^{21}$ cm^{-3} (0.32 hole/Cu atom) and then decreases with further increase of the hole concentration. Thus, for both the systems a correlation between the carrier concentration and superconductivity transition temperature exists. The suppression and disappearance of superconductivity in the heavily doped region is one of the characteristic features of all cuprate superconductors [29].

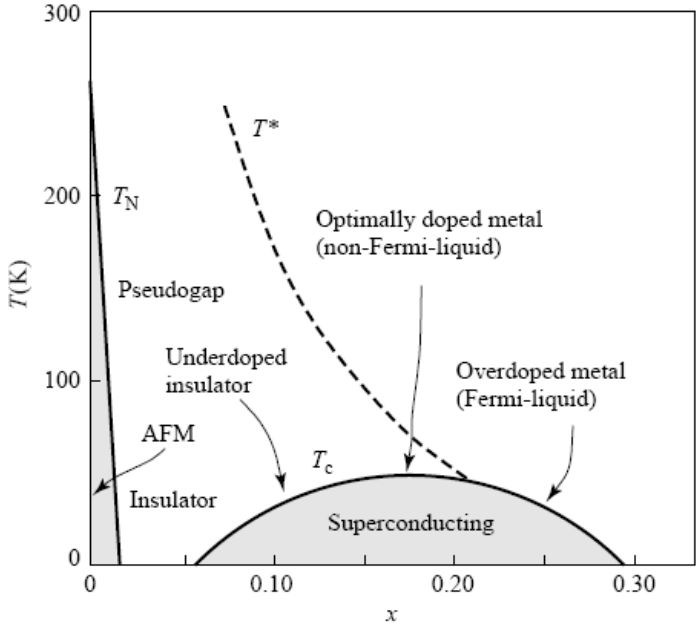

Figure 5. Typical phase diagram with doping in cuprate superconductors. (AFM= antiferromagnetic phase)

How doping is achieved, i.e. how the parameter x on the horizontal axis of Fig. 5 is controlled, depends on the compound. In the case of the La-based, original high-T_c materials, the key is to replace trivalent La with divalent Ba or Sr. Because the basic compound La_2CuO_4 is charge neutral, replacing La^{3+} with Ba^{2+} and still demanding charge neutrality results in a freed positive charge, donated to the valence band. On the other hand, in the case of oxygen depletion, removing an oxygen atom leaves behind two incomplete bonds, which upon completion free two positive charges, or holes.

The substitution of rare-earth ions for Ca was found to affect the transport and magnetic properties as well as the hole carrier concentration in BSCCO compounds.

Kishore et al. [30,31] studied the superconducting and normal state properties of the $Bi_{1.7}Pb_{0.3}Sr_2Ca_{2-x}Y_xCu_3O_y$ ($0.0 \leq x \leq 0.1$) system and they found that Y

substitution promotes the conversion of the major (2223) phase to (2212) phase. The solubility limit of Y in the BSCCO (2223) system is reported to be around x = 0.02. Samples with higher Y contents have shown a two step inductive transition which they believed indicates the presence of the two phases. They concluded that Y substitution decreases the hole carrier concentration both in the 2223 and 2212 phases with an increased electron phonon interaction at low temperatures. They also found that T_c value decreased with Y substitution. The lattice parameters do not vary much in the high T_c 2223 phase. The *c* parameter of the low T_c phase, however, decreases with increasing Y concentration. They concluded that the decrease in *c* parameter indicates Y is substituting the Ca ion in the 2212 phase. The superconducting transition width ΔT_c increases with increasing x which indicates that the samples became more and more inhomogeneous. Small second steps are seen in R-T curves for the doped samples. They believe that these steps are due to the intragrain coupling in the 2223 phase. They verified that for an optimum hole concentration, T_c is maximum and above and below this optimum value the T_c decreases. They attribute the degradation of the superconducting properties to the decrease in hole concentration. They found similar results for the Gd substituted sample, but the rate of suppression for T_c is more for the Gd substituted sample. They claim this to be due to the magnetic nature of Gd, which contributes to the pair breaking mechanism.

Kanai et al. [32] investigated the effect of 34 dopants on the BSCCO system. They found that dopants of rare earth family (Yb, Ce,Y, Sm and La) substitute into the Ca site and resulted in the disappearance of the high-T_c phase and the increase of the onset T_c's in the low-T_c phase.

Ilonca et al. [33] investigated the effect of partial replacement of Ca by Y, Er and Lu on the structural and transport properties of $(Bi_{1.6}Pb_{0.4})(Sr_{1.8}Ba_{0.2})(Ca_{1-x}R_x)_2Cu_3O_y$ superconductor ceramics ($0 \leq x \leq 0.03$). The substitution of Y, Lu and Er at the Ca site induced the decrease of the volume fraction for the 2223 phase and the increase of the 2212 and 2201 phases volume fractions. They observed a linear dependence of resistivity on temperature in the normal state. They observed nearly the same rate of depression of the T_c for all of these substitutions. They attribute the T_c suppression to the increase of oxygen content in Bi_2O_2 double layers with increasing Y, Lu and Er concentrations. They conclude that the excess of positive charge for RE^{3+} causes repulsion between the CuO_2 layers so that the CuO_2-CuO_2 plan seperation increases. The increase in rare earth concentration induce excess oxygen incorporated between the Bi_2O_2 double layers [34].

Kishore et al. [35] also studied the transport and magnetic properties of $Bi_{1.7}Pb_{0.3}Sr_2Ca_{2-x}Sm_xCu_3O_y$ ($0 \leq x \leq 2.0$). From the X-ray diffraction (XRD) data they found that with Sm substitution, the volume fraction of (2223) phase decreases and the compounds with $x > 0.05$ show only the (2212) phase. With increasing Sm content, T_c value, the superconducting volume, and the hole carrier concentration also decrease.

It is well known that superconductivity is suppressed by the presence of magnetic ions in the conventional metallic superconductors. This behaviour can be understood in terms of the pair-breaking mechanism.

Öztürk et al. [36] investigated the effect of the partial substitution of Ca by Sm in the Bi-2223 superconducting samples prepared by standard solid-state reaction method. They found that increasing the Sm content shifted the superconducting

transition temperature (T_c), activation energy (U_0), and the irreversibility temperature to lower values. They interpreted the lower zero resistance transition temperature with increasing Sm content as a result of the suppression of superconductivity by the Sm^{3+} ions. They claim that the broader transition of Sm substituted samples indicates presence of impurities and weak-links between superconducting grains. The transition from normal to the superconducting state for Sm substituted samples has double step nature. They believe that the double step resistive transition is an indication of weak-links. As the Sm content increases, they observed much broader superconducting transitions, higher room temperature resistivities and lower critical transition temperatures. They claim that the substitution of Sm leads to weakening of the coupling of the grains and deterioration of the microstructure and superconducting properties of the samples. They observed that the lattice parameter *c* decreases significantly with increasing Sm content. They explain the behaviour of lattice parameter by the increase of the oxygen content in the unit cell by the replacement of Ca^{2+} by Sm^{3+} in the structure. They speculate that the excess of oxygen goes into the bismuth oxide layers causing a decrease in lattice parameter *c*. They also comment on the possibility of the decrease of lattice parameter *c* due to incorporation of Sm ions into the interstitial sites in the unit cell rather than occupation of the Ca sites. As a last possibilty, they explain the decrease of *c* parameter with Sm addition due to the difference in the cationic radii of Sm^{3+} (0.96 Å) replacing Ca^{2+} (0.99 Å).

Terzioğlu et al. [37] investigated the effect of substitution of Sm for Ca on the

superconducting, microstructure and mechanical properties of $Bi_{1.6}Pb_{0.4}Sr_2Ca_{2-x}Sm_xCu_3O_y$. Superconducting and mechanical

properties degrade similarly with increasing Sm content [38]. It was also reported that for x=1.0 and 1.5 the samples show semiconducting behavior. For higher values of Sm content ($x \geq 0.1$), only the Bi-2212 phase can be observed. Critical current density and SEM measurements show weak-link in the intergranular region of the samples. The surface morphology of the samples degrade with increasing Sm doping. They suggest that the substitution of Ca^{2+} by the rare earth Sm^{3+} provides an additional electron, which, in turn, decreases the hole carrier concentration which leads to a decrease of T_c and J_c.

Yeğen et al. [39] investigated the magnetic properties of Sm doped Bi-2223 superconductor by Hall probe ac susceptibility method at low magnetic fields. They found that the T_c reduced upon Sm doping and they claimed that that this was due to the modification of the crystallographic structure of the Bi-2223 phase. The increase in Sm content weakens the flux pinning. Increasing Sm content results in the appearance of low temperature phase and peaks of the high temperature phase diminish in the XRD measurements. The lattice parameter c decreases with increasing Sm content. They attributed the decrease of c parameter to Sm substitution for Ca in the crystal structure

Kishore et al. [40] investigated the $Bi_{1.7}Pb_{0.3}Sr_2Ca_{2-x}Gd_xCu_3O_y$ system for different concentrations of Gd (x=0, 0.01, 0.05, 0.075, and 0.1). Substitution of dilute quantities of Gd^{3+} for Ca^{2+} is found to change the superconducting properties of the system drastically. The volume fraction of the high T_c 2223 phase present in samples without Gd^{3+} (x = 0) vanishes even for x = 0.01. Unlike Sm, even the Gd concentration as low as (x=0.01) suppresses the high T_c phase completely. For all the doped samples, they could not obtain a value of T_c offset above 77 K. With

increasing concentration of Gd the onset temperatures decreases drastically even for very diluted concentrations. The T_c onset obtained from χ'_{ac} versus *T* decreases from 109 to 74 K for x = 0 to 0.1, whereas the loss peak from χ''_{ac} versus *T* decreases from 108 to 56 K for x = 0 to 0.05. They report the same behavior for resistance measurements. They compare the results with their previous work with Sm doping and report that the doping of Gd degrades superconducting properties of BSCCO-2223 system more drastically.They explain the results on the basis of a possible variation of hole concentration with trivalent rare earth ion substitution and also on the basis of the magnetic nature of the substituted ions. They also observed that the T_c suppression rate is more in Sm substituted system as compared to Y-substituted system indicating that the magnetic nature of the ion also contributes to the lowering of T_c to a certain extent [30,41].

Mishra [42] studied the effects of Gd doping at calcium site into the Bi-2223 system. He found that Gd substitution caused a decrease in the carrier concentration. The presence of low concentrations of gadolinium ($x < 0.8$) at calcium site did not inhibit the growth of (Bi, Pb)-2223 phase. No significant change in the lattice parameters of the (Bi, Pb)-2223 phase is reported. However, the normal state resistivity behaviour and $T_c(R = 0)$ values confirmed the Gd substitution in these specimens. The rate of decrease of T_c (R=0) values in Pr-substituted (Bi, Pb)-2223 is roughly 5 K/(%Pr) [43] as compared to 12 K/(%Gd) in Gd-substituted (BiPb)-2223. He explains the difference due to the smaller ionic radius of Gd^{3+} compared to the ionic radius of Pr^{3+}. Therefore, Gd has higher solubility in (Bi,Pb)-2223 as compared to Pr, and is, more detrimental to the superconductivity. Gd is a magnetic f-band element with high net magnetic moment. Gd, therefore, like other magnetic impurities,

disturbs the antiferromagnetic ordering in Cu-O planes and leads to pair-breaking effects near the Fermi level [44].

Ekicibil et al. [45] analyzed the effect of Gd doping into the BSCCO superconductor. They found that with increasing Gd^{3+} doping for Pb^{2+} the (2223) phase gradually transforms into the (2212) phase and J_c decreases with increasing Gd concentration. With incresing concentration of doping, a monotonic decrease of *c*-parameter with a simultaneous small elongation of the *a*-parameter is observed.

Sangeetha et al. [46] reported studies on $Bi_{1.7}Pb_{0.3}Sr_2Ca_{1-x}Gd_xCu_2O_8$ compounds in which Ca^{2+} is replaced with different concentrations of Gd^{3+} ion. They observed that the structural parameters, oxygen content and hole carrier concentration change with Gd concentration. Their calculation of the lattice parameters show that the *c* parameter decreases and the *a* parameter increases with increasing Gd content. The decrease in the *c* parameter is attributed to substitution of smaller Gd ion in place of the larger Ca^{2+} ion. Their results exhibit superconductivity in the $0.0 \leq x \leq 0.4$ concentration range and for higher concentration of Gd, they become insulating. Both transport and magnetic properties confirm metal–insulator transition in the $x>0.4$ region. They report that with increasing Gd content the hole concentration decreases while the resistivity increases.

Biju et al. [47] studied the effect of substitution of the rare earth ion Gd at Sr site of (Bi, Pb)-2212 superconductor by varying Gd in the stoichiometric level. They report the increase of both the critical temperature T_c and critical current density J_c with Gd substitution at Sr site, and the maximum T_c is observed for $x = 0.3$ in the initial composition $Bi_{1.7}Pb_{0.4}Sr_{2-x}Gd_xCa_{1.1}Cu_{2.1}O_y$ and the maximum J_c for $x = 0.2$. The results show that Gd substitution at Sr site favors the growth of (Bi, Pb)-2212.

They observed no secondary phases including Gd or other cations in XRD figures, so they conclude that Gd^{3+} ions enter into the Sr site of (Bi,Pb)-2212. From SEM measurements, the grain sizes are seen to decrease as the Gd content increases. As Gd substitution increases, normal state resistivity of the samples increases. They report that this indicates the decrease in the amount of charge carriers.

Gao et al. [48] studied the superconducting properties of Y, Gd and Pr doped Bi-2212 superconductors. All three dopants substitute a trivalent ion for divalent Ca and cause a depression of T_c observable in the resistivity and susceptibility measurements. Both Pr and Gd retain their free-ion magnetic moment and appear to cause little, if any, magnetic pair breaking. Instead, the dominant suppression mechanism in all three cases is driven by the filling of the Cu hole by the extra electron.

Zhao et al. [49] produced Gd doped Bi-2212 single crystals and examined the superconducting properties. The *c* axis length decreased gradually with Gd doping. This reduction is explained by two reasons. Firstly, smaller ionic size of Gd^{3+} replacing Ca^{2+} and secondly, the oxygen content in the system increases with Gd concentration for high valence cation substitution. The T_c of the crystals increases slightly at first and then decreases rapidly upon Gd doping.

Sedky [50] studied the influence of rare-earth substitution for Ca in (Bi, Pb)-2212 superconducting system. $Bi_{1.7}Pb_{0.3}Sr_2Ca_{0.50}R_{0.50}Cu_2O_y$ samples with various R (R = Y, Gd, Nd and La) are prepared by using solid-state reaction method. He made measurements on the superconducting and mechanical properties and found that the Vickers microhardness gradually decreased with various R as one moves towards the right hand in lanthanide series. The on-set temperatures are found as 87 K for pure

sample and it decreased to 80, 68 and 36 K for Y, Gd, and Nd samples, respectively. They report that the sample with La did not show superconductivity. The carrier concentration is found to decrease with various R. From XRD measurements the maximum intensity I_{max} of 2212 phase decreases with various R from up to La sample and vice versa for 2201 phase. They report the reason for this as the substitution by higher ionic size of R that decreases the intergranular contacts and leads to decreasing the formation of Bi-2212 phase in this type of samples. From both XRD and SEM results they claim that the majority of R enters into the Ca site and due to the lack of impurity phases. From the comparison of T_c values for the samples, they conclude that the solubility of R^{3+} in (Bi, Pb)-2212 system decreases with increasing ionic radius of R, as one move towards right in lanthanide series. From these results they believe that the T_c depression is mainly controlled by the amount of excess oxygen which is mainly considered the main factor for controlling the carrier concentration by cation substitution in this type of Bi-2212 superconducting system.

Koike et al. [51] investigated the correlation between superconducting T_c and hole concentration in the $Bi_2Sr_2CaCu_2O_{8+\delta}$ system. The hole concentration is varied by substituting cations with different valences for Sr or Ca. In order to increase the hole concentration, some samples were annealed at 430°C in 250 bar of oxygen pressure. They found that T_c increases, takes a maximum at the hole concentration corresponding to 0.2–0.3 holes per CuO_2 unit, and then decreases, with increasing hole concentration.

Structure, resistivity and susceptibility have been studied in the $Bi_2Sr_2Ca_{1-x}RE_xCu_2O_{8+\delta}$ (RE=Nd and Pr) system. The samples with $0 \leq x \leq 1$ have a

single phase of the $Bi_2Sr_2CaCu_2O_{8+\delta}$ structure. The oxygen concentration, $8+\delta$, is estimated as about 8.3 which is independent of the RE composition x. The T_c increases slightly with x in the range of $x \leq 0.10$ and remains constant at about 85 K for $0.10 \leq x \leq 0.25$, then decreases linearly with x for $0.25 \leq x \leq 0.55$. Superconductivity disappears for the samples with $x \geq 0.55$ in both cases. From the susceptibility data, they reported that Nd and Pr ions in the samples are both trivalent. They claim that the hole concentration in [Cu–O] plays a most significant role in the occurrence of superconductivity in the Bi–Sr–Ca–Cu–O system [52].

In the above literature, when Gd is added to Bi-2223 phase, the superconducting properties especially T_c decreases. When Gd is added to Bi-2212 phase, there are conflicting results which report decrease of superconducting properties and also there are others in which the superconducting properties increase. This difference of behaviours for the two phases can be explained by the difference of hall concentration limit of the two phases. For Bi-2212 phase, the superconductivity is within the $(0.25 \leq x \leq 0.35)$ limit but for the Bi-223 phase the optimum value of hole density is in a small neighborhood of x=0,20. For 2223 phase even a small difference from the optimum value causes the superconducting properties to decrease [28].

There are conflicting results whether the dominant reason for the changes on the superconducting properties upon doping by rare earths is due to magnetic effects or due to the change in hole concentration. It is clear from the measurements and discussions presented here that the effect of impurity doping on the physical properties of high-temperature superconductors is far from clear-cut. In particular, the addition of magnetic impurities may not cause the significant changes one

may expect from a simple examination of the free-ion moments. More future work and results are needed for a better understanding of these mechanisms.

CHAPTER 4

EXPERIMENTAL TECHNIQUES

4.1 SAMPLE PREPARATION

The effect of Gd addition into BSCCO-2223 system is studied in this work. The Gd added $Bi_{1.8}Pb_{0.35}Sr_{1.9}Ca_{2.1}Cu_3Gd_xO_y$ samples with x = 0, 0.2, and 0.4 were prepared by the standard solid-state reaction method using high purity chemicals Bi_2O_3 (99.99%), PbO (99.9+%), $SrCO_3$ (99.9+%), $CaCO_3$ (99+%), CuO (99+%) and Gd_2O_3 (99+%). These oxides and carbonates were weighed with a precision microbalance.

The following balancing equation is used to calculate the appropriate amounts of chemicals.

Chemical equation:

$$(0.9)Bi_2O_3 + (0.35)\ PbO + (1.9)\ SrCO_3 + (2.1)\ CaCO_3 + (3)\ CuO + (x/2)\ Gd_2O_3$$

$$\rightarrow\ Bi_{1.8}Pb_{0.35}Sr_{1.9}Ca_{2.1}Cu_3Gd_xO_y$$

	Bi_2O_3	PbO	$SrCO_3$	$CaCO_3$	CuO	Gd_2O_3
Molecular weights(g/mol)	465.96	223.19	147.63	100.09	79.55	362.5

Table 1. Molecular weights of the chemicals used.

Then they are mixed in a grinding machine for 24 h. Since homogeneity and quality of the samples is connected to the mixing and grinding processes, this step is

important for the quality of the samples.

4.2 HEAT TREATMENT

After milling, the mixed powders were subjected to a three-stage calcination process in air at different temperatures (700, 750 and 800 ^{o}C for 24 h). Following every calcination stage, the mixture was cooled to room temperature and ground. Intermediate grinding are done to improve phase purity by obtaining more homogeneous samples.

4.2.1 CALCINATION

Calcination is the first stage of heat treatment of the starting powder which is done at lower temperatures than sintering. Calcination releases the carbon in the starting powder and carbonates decompose to metal oxides. Better superconducting properties are obtained when calcined powder is used. If the initial raw powder is directly sintered at higher temperatures without calcining, the volatile elements (Pb and Bi) may be lost and excessive melting may occur. This causes significant changes in the chemical composition which degrades the formation of the desired phases. Also some elements may form impurity phases [10].

4.2.2 SINTERING (ANNEALING)

Sintering is a method for making objects from powder, by heating the material below its melting point (solid state sintering) until its particles adhere to each other. Sintering is traditionally used for manufacturing ceramic objects, and has

also found uses in such fields as powder metallurgy.

Superconducting properties are related to the annealing temperature and phase formation. J_c increases with increasing sintering temperature, reaching a maximum at a certain annealing temperature just below the temperature at which the sample begins to melt. At optimum annealing temperature, large grain sizes will be obtained. Melting the samples reduces J_c probably due to the second phase precipitated at grain boundaries during the solidification process. The optimum annealing temperatures of the three superconducting phases of the Bi-based system are 820°C (2201 phase), 850-860°C (2212 phase), and 870-880°C in air when there is no Pb addition to 2223 [53].

The phase formation is limited to a certain temperature range which is close to the melting point of that particular compound. A temperature just below the softening of the specimen is selected as the appropriate annealing temperature. If Pb is added to 2223, the optimum annealing temperature changes. Semiconducting-like R-T curves are obtained for 2223 samples if the annealing temperature is higher than optimum, for instance the 2223 phase decomposes into the 2212 phase and Ca_2CuO_3 after being heat treated at 865°C [54]. This shows that a liquid layer forms in some regions of the grain boundaries and eventually becomes a semiconducting layer. The optimum annealing temperature decreases with increasing Cu and Pb content [55]. The size of pores increases with increasing heat treatment temperature [56].

Annnealing time is another important parameter. Generally, long annealing times are needed to form large volume fraction of 2223 phase. It also affects the width of transition. Shorter annealings result in broader transitions. Annealing times longer than optimum may also cause loss of volatile elements.

After completing the calcination process, the powder material was pelletized into rectangular bars of 10x4x2 mm^3 at 300 MPa with a manual hydraulic press. Pressing increases the density of the samples and the connection surface area of the grains. This reduces weak links.

The pellets were sintered in air at 830 ^oC for 48 h and then cooled down to room temperature. The heating and cooling rates were chosen to be 10 and 3 ^oC min^{-1}, respectively (Fig. 6). The calcinations and annealing processes of the samples were carried out using a programmable tube furnace (PROTHERM-Model PTF 12/75/200). The temperature profile of this furnace was previously analyzed and calibrated with a thermocouple. For comparison, an undoped sample was also annealed under the same conditions. The prepared samples with different Gd additions of x = 0, 0.2, 0.4, in $Bi_{1.8}Pb_{0.35}Sr_{1.9}Ca_{2.1}Cu_3Gd_xO_y$ will be hereafter denoted as Gd0, Gd2, Gd4 respectively. The preparation route of the samples is schematically drawn in Fig. 7.

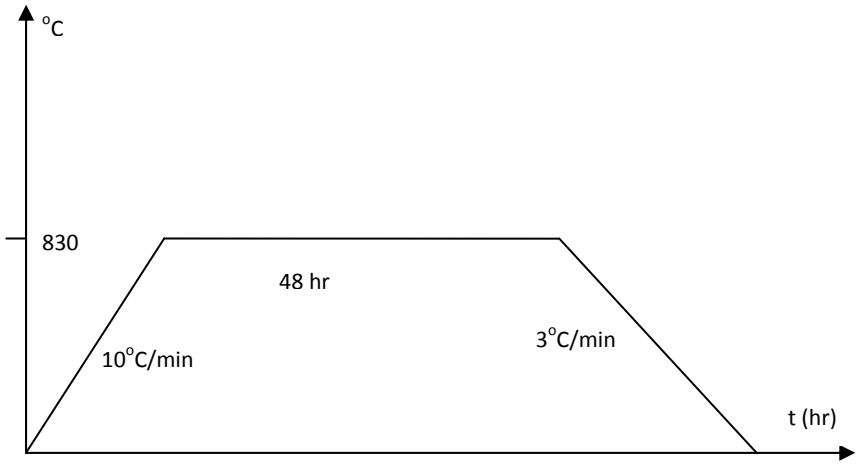

Figure 6. Diagram of the sintering process

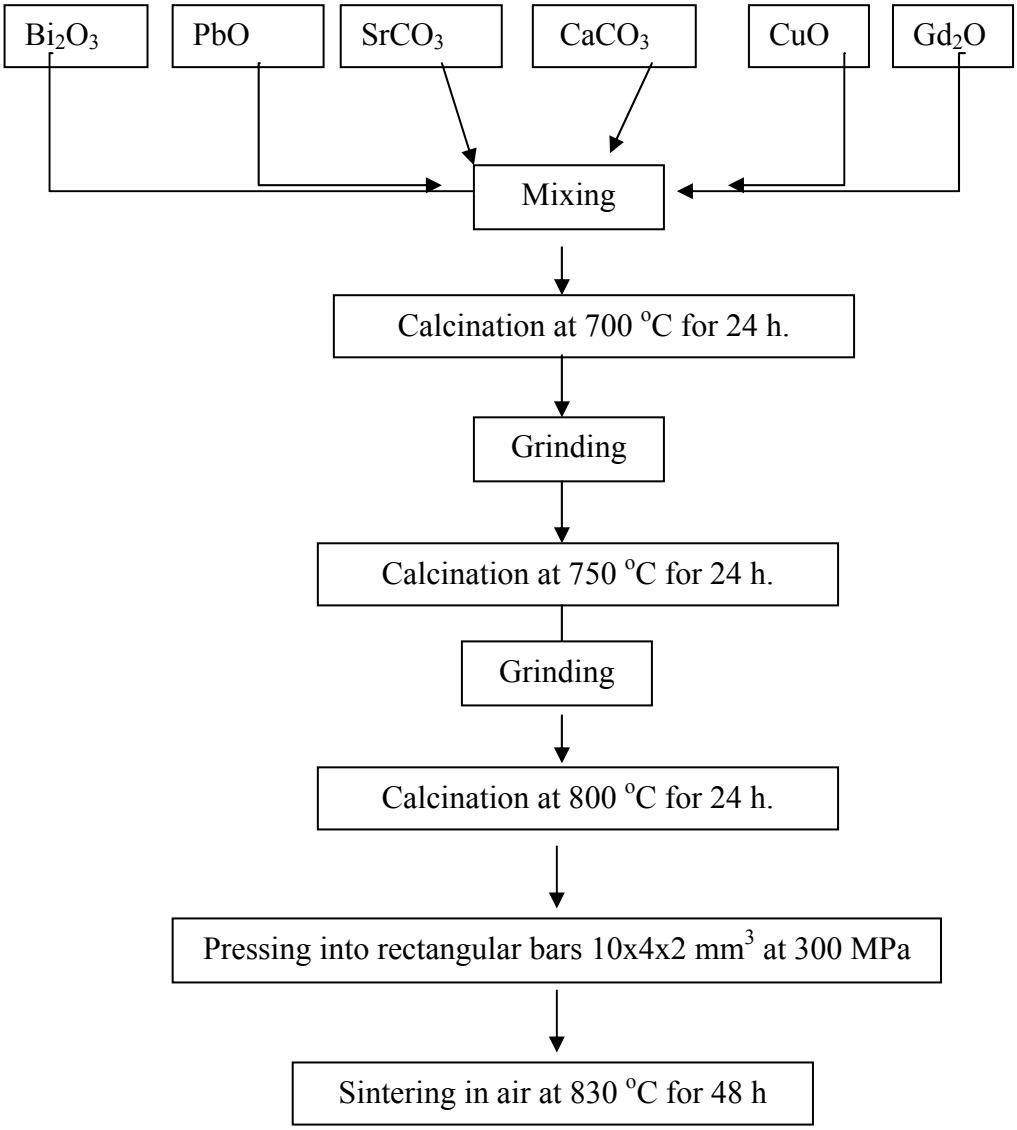

Figure 7 . Preparation route of the samples.

4.3 CHARACTERISATION OF THE SAMPLES

The electrical resistance R of an object is defined as the ratio of the voltage V and current I between two points of a conductor. So the direct way of measuring resistance of an object is to measure these two magnitudes; current and voltage. As the resistance of the contacts becomes comparable to sample resistance, it becomes necessary to separate the contacts conducting the current from the contacts between which the voltage is measured, in order not to include contact resistance into the resistance of the sample. This is the rule when measuring resistivity of semiconducting materials, and also when measuring very small resistances of good conductors.

A four-point resistivity measurement may be described as the measurement of voltage drop between a pair of probes contacting the specimen by making the current to flow through a second set of probes, namely the source and sink contacts, respectively. This scheme essentially allows for measuring the true specimen resistance without including the contact resistance between the probes and the specimen. This is made possible by making the voltage probes part of a high impedance circuit, thus allowing only negligible current to flow through this circuit [57].

The most common way of measuring the resistivity of a material is by using a four-point collinear probe. This technique involves bringing four equally spaced probes in contact with a material of unknown resistance. The probe array is placed in the center of the material, as shown in Fig. 8.

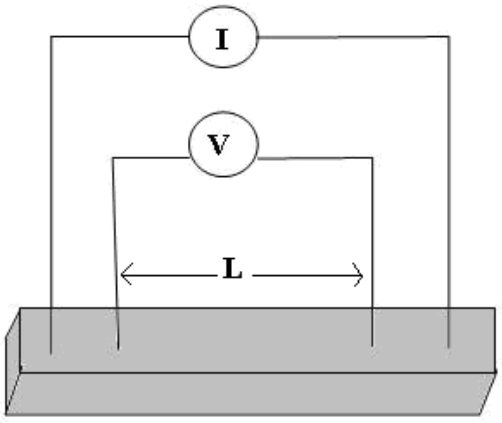

Figure 8. Drawing of the connections in a transport measurement. The inner two contacts are used to measure the potential difference which is related to resistance. Current is supplied from the outer two contacts.

The two outer probes are used for sourcing current and the two inner probes are used for measuring the resulting voltage drop across the surface of the sample. With the known current and measured voltage, resistivity is calculated as follows:

$$R=\rho.L/A \quad \text{and} \quad V=I.R \tag{3}$$

$$\rho=R.A/L = (V/I).(A/L) \tag{4}$$

where ρ is the resistivity, L is the distance between the inner contacts, and A is the cross sectional area of the sample.

4.3.1 R-T MEASUREMENTS

To observe the transition of a superconductor to the superconducting state, measurement of resistance versus temperature is the standard method for transport measurements. In this method, a constant small test current is driven from the outer

contacts through the sample and the potential difference between the inner two contacts is measured and recorded while the temperature of the sample is changed in a cryostat. While the temperature decreases, a linear decrease of resistance until the onset critical temperature is observed for most superconductors. At the onset critical temperature, the resistance begins to drop sharply. This shows that at least one resistanceless path is established between the voltage contacts of the sample. At offset critical temperature the resistance is measured as zero within the accuracy of the voltmeter. With this method, a superconductor can be characterized.

In this work, the measurements of dc resistivity were performed on all samples with the four-probe method. Both voltage and current contacts were made with silver paint. We measured temperature (40 K-130 K) dependence of resistivity of the samples running 5 mA dc current through the samples in the cryostat. A Keithley 220 programmable current source and a Keithley 2182A nano-voltmeter were used for the resistivity measurements. The transition temperature, T_c, was defined as zero resistivity critical transition temperature within the sensitivity of our measurement system.

4.3.2 I-V MEASUREMENTS

To find the maximum current passing through a sample or critical current density of a sample, the potential difference between the inner contacts is measured and recorded while the current applied to the sample is gradually increased at constant temperature. For currents under the critical value the potential difference is zero. When the critical value is reached, the potential difference (resistance) begins to increase. For consistency with the literature, a criterion has to be adopted for determination of the critical value of current. For the calculation of critical current

density, the potential difference values are divided by the distance between the inner contacts and the current values are divided by the cross sectional area of the sample. So a relation between Volts/cm versus current density J_c is obtained. The dimensions of the samples were carefully measured with a micrometer to calculate the cross-section and the length between the contacts. Since the samples are rectangular, this was a simple process.

The measurements of transport critical current density, J_c, were performed on all samples with the four-probe method. We determined J_c from the I-V curves at 77 K in liquid nitrogen dewar, the criterion used for critical current was $1\mu V/cm$. Actual dc currents up to 5 A were passed through the samples. Resistive contacts caused heating and the tests were completed in possible shortest time to reduce this effect. A Keithley 220 programmable current source and a Keithley 2182A nano-voltmeter were used for I-V measurements.

4.3.3 XRD MEASUREMENTS

X-ray diffraction (XRD) data were taken using a Rigaku D/Max-IIIC diffractometer with CuK_α radiation in the range $2\Theta = 5°- 60°$ with a scan speed of 3°/min and a step increment of 0.02° at room temperature. XRD measurements provide data about lattice parameters for Gd added Bi-2223 bulk samples. Phase purity and the lattice parameters were determined from these XRD results. The accuracy in determining the lattice parameters *a* and *c* was ± 0.001 Å .

The (002) peaks are mostly used to characterize these phases because they can be clearly separated for each phase and they do not overlap with the impurity phases of this system. In Table 2, the reflection parameters of BSCCO system are shown, and in Fig. 9, the XRD reflection patterns are shown.

h	k	l	2201	2212	2223
0	0	2	7.24	5.75	4.75
0	0	4	14.50	11.50	9.50
0	0	6	21.83	17.29	14.28
0	0	8	29.24	23.13	19.07
0	0	10	36.79	29.02	23.91
1	1	3	25.75	24.86	24.37
1	1	5	29.68	27.47	26.21
0	0	12	44.50	35.00	28.78
1	1	7	34.81	31.01	28.77
1	1	9	40.77	35.22	31.88
2	0	0	33.15	33.15	33.15
0	0	14	52.43	41.07	33.71
1	1	11	47.34	39.94	35.43
0	0	16	60.65	47.27	38.71
1	1	13	54,40	45.06	39.32
1	1	15	61.93	50.50	43.48
0	0	18	69.22	53.62	43.78
0	2	12	56.60	48.97	44.46
2	2	0	47.59	47.59	47.59
1	I	17	69.93	56.24	47.88
0	0	20	78.26	60.15	48.94

Table 2. XRD reflection angles for BSCCO system (taken from reference 10).

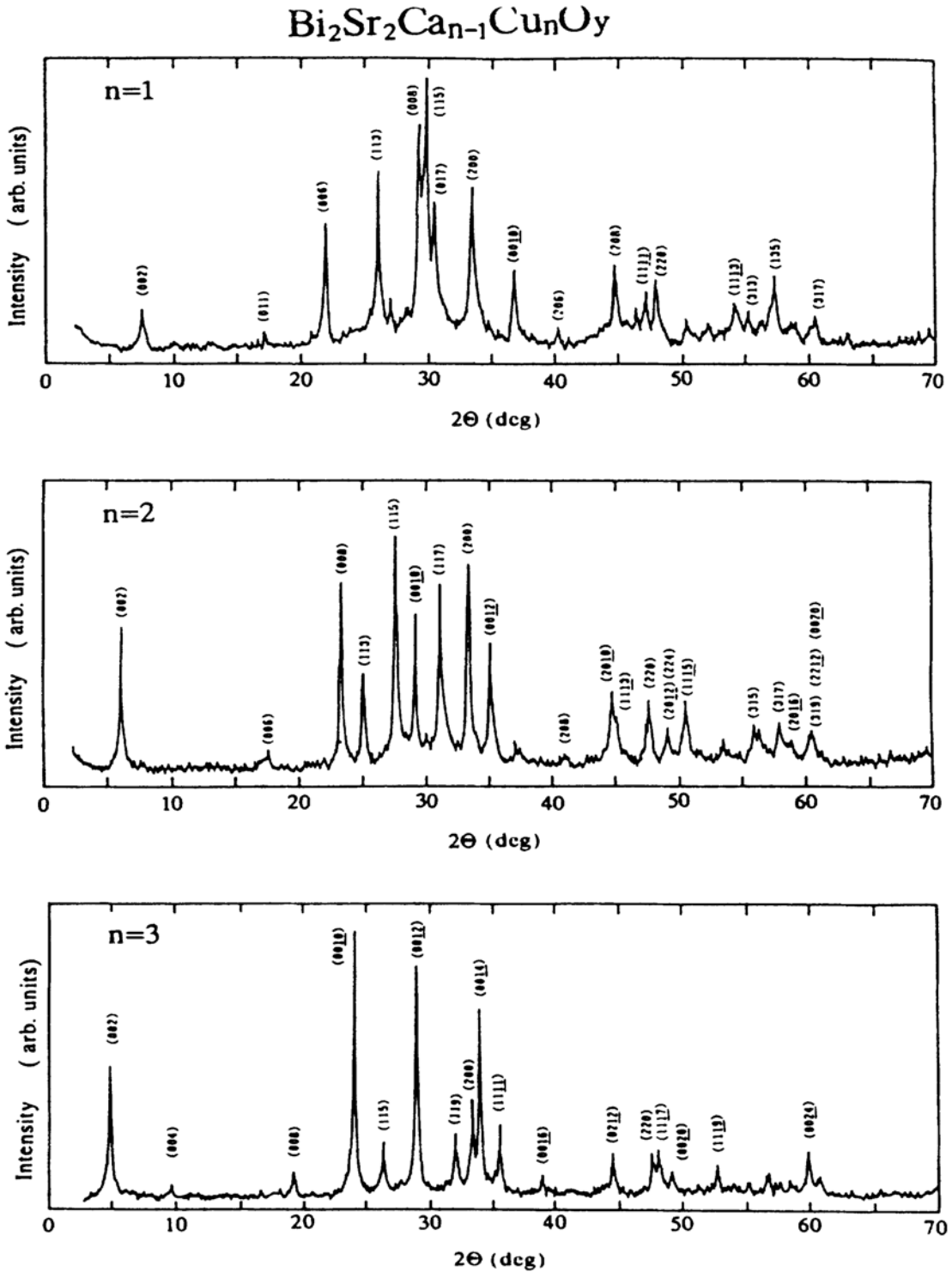

Figure 9. Typical X-ray diffraction pattern for nearly single phase samples of the n=1 (2201), n=2 (2212), and n=3 (2223) samples.

4.3.4 SEM MEASUREMENTS

Microstructure examination of the samples was done using a Philips XL30 SFEG scanning electron microscope. SEM examinations were performed on free outer surfaces of the bulk samples. SEM examinations give information about grain alignment, grain size and porosity of the samples.

4.3.5 MICROHARDNESS MEASUREMENTS

The mechanical properties of the samples by load dependent and independent Vickers hardness measurements have been carried out to assess the effects of Gd addition.

To investigate the effect of Gd addition on the mechanical properties of the samples, we measured the diagonal length as a function of test load. Conventional Vickers microhardness measurements consist of applying a load F on the test material via a geometrically defined indenter and after the indenter is removed, measuring the characteristic dimension d of the resultant impression.

Hardness measurements of BSCCO samples were performed on the polished surface of the examined samples with a digital microhardness tester (Instron Series 2100) at room temperature. All samples were polished prior to being tested. The applied load, F, was varied from 0.245 to 2.940 N and the applied time was 10 s for all trials, and the diagonals of indentation were measured with an accuracy of ± 0.1 μm. Indentations were made at different parts of the samples' surface in such a way that the distance between any two indentations was no less than two times the diagonal of the indentation mark to avoid surface effects due to neighboring

indentation. An average of five readings at different locations of specimen surfaces was taken to obtain reasonable mean values for each load.

CHAPTER 5

RESULTS AND DISCUSSION

To investigate the effect of Gd addition on the superconducting properties of the samples, we performed dc electrical resistivity measurements. The electrical resistivity was measured using the standard four-probe dc technique, in the temperature range between 40 and 130 K. Fig. 10 shows the temperature variation of the resistivity of pure Gd0 and Gd added samples Gd2, and Gd4.

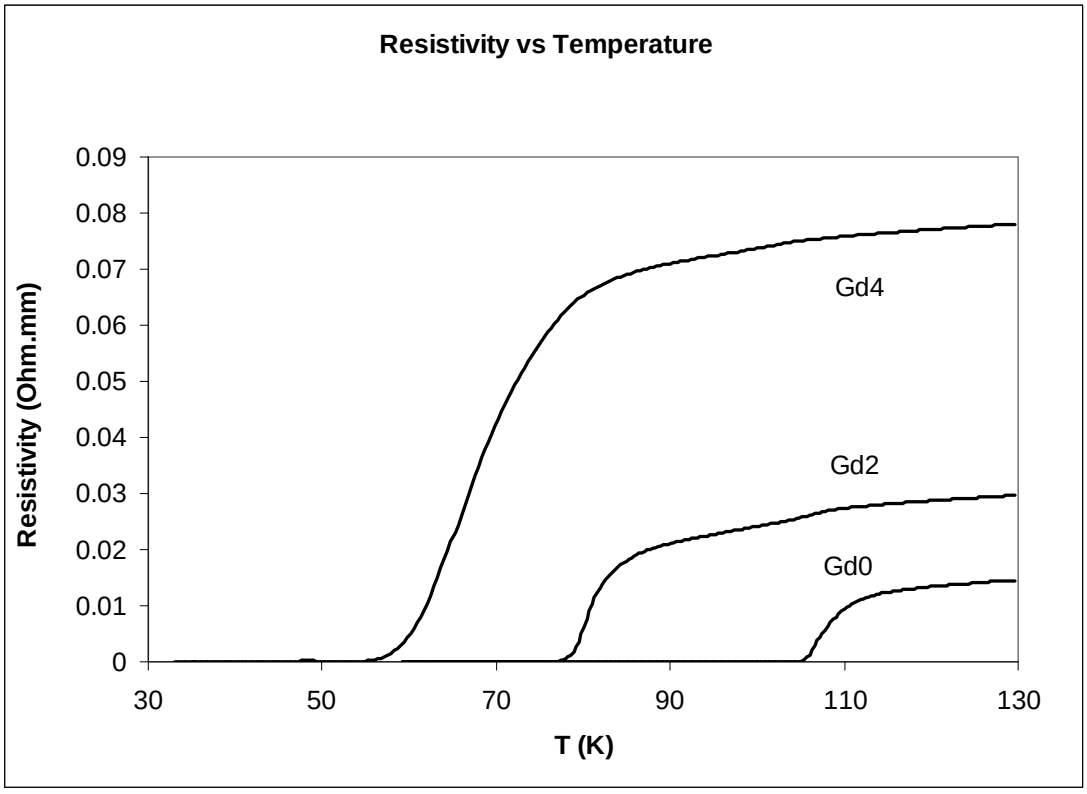

Figure 10. Resistivity as a function of temperature for Gd0, Gd2 and Gd4 samples.

Zero-resistivity transition temperatures of the Gd0, Gd2, Gd4 samples are determined as 105 K, 77 K, and 55 K, respectively. The T_c values decreased with increasing Gd addition. The critical temperature of high-T_c superconductors depends on the density of mobile holes in the CuO_2 planes and thus on the average Cu valance [58]. The replacement of Ca^{2+} ion by Gd^{3+} ions leads to a decrease in the Cu valance [59, 60], whereas, the substitution of Pb^{2+} in Bi^{3+} site increase Cu valance [61]. As a result, thus T_c is expected to decrease with increasing Gd content. There are a few researches on the effects of rare earth ion additions or substitutions in the Bi-2223 superconductors. Some researches [62, 63] investigated the effect of Gd substitution for Ca and observed that Gd^{3+} ion depressed the superconducting transition temperature as it is in this study. The observed decrease of T_c for our samples makes the substitution at the Ca site more likely. As can be seen from Fig. 10, Gd added samples showed a broad transition, which indicates presence of impurities and weak-links between superconducting grains. Broadening of the transition width and appearance of double step behaviour indicate that the Gd added samples have more numerous grain boundaries since the double step resistive transition is indication of weak links. Offset critical temperatures on the other hand, exhibit resistive tails at lower temperature end of the R-T curves which is direct consequence of granular microstructure evidenced by grain size calculations.

It is observed that the zero resistivity transition temperature of the Gd0 (105 K) is higher than those of the Gd added samples. This is consistent with previous works given at the preceding chapter. The results obtained from the dc resistivity as a function of temperature measurements are given in Table 3. Room temperature resistivities were also calculated from room temperature I-V curves for all samples and tabulated in Table 3. The room temperature resistivity value of all

samples increased with increasing Gd addition, which agrees with previous works. The lower zero resistance transition temperature with increasing Gd content could be interpreted that the presence of more non-superconductive phases arising from the suppression of superconductivity by the Gd^{3+} ions. As the Gd addition increases, much broader superconducting transitions and higher room temperature resistivities were observed. This degradation can be attributed to the modified grain boundary properties by Gd content [64].

Sample	Tc_0 (K)	Tc Onset(K)	ΔT (K)	ρ at 294K (mΩ.cm)	a (Å)	c (Å)	Unit Cell Volume (Å^3)	Phase ratio (2223/2212)
Gd0	105	114	9	2.456	5.416 (H)	37.206 (H)	1091.37	92/08
					5.415 (L)	30.715 (L)	900.63	
Gd2	77	89	12	4.297	5.424 (H)	37.144 (H)	1092.77	07/93
					5.433 (L)	30.629 (L)	904.09	
Gd4	55	88	33	8.602	5.461 (L)	30.554 (L)	911.20	0/100

Table 3. Results of XRD and resistivity measurements of the samples. Note that in the phase ratio calculations only the peaks of the 2212 and 2223 are taken into account.The impurity phases are not considered.

It is well known that a parabolic relationship holds between the transition temperature and the carrier concentration, *p*. The carrier (number of holes per Cu atom) concentration, *p*, is calculated by using the relation [9]

$$T_c/T_c^{max} = 1 - 82.6\,(p - 0.16)^2 \qquad (5)$$

where T_c^{max} is taken as 110 K and 85 K for Bi-2223 and Bi-2212 systems, respectively. This formula is applicable to several doped cuprate superconductors.

Previous calculations for the undoped or unsubstituted Bi-2223 had shown that the values of *p* ranged from 0.116 to 0.160. So the *p* in the underdoped and overdoped regions can be determined by using the following equations respectively;

$$p = 0.16 - \left[\left(1 - \frac{T_c}{T_c^{\max}}\right)/82.6\right]^{1/2} \tag{6}$$

and

$$p = 0.16 + \left[\left(1 - \frac{T_c}{T_c^{\max}}\right)/82.6\right]^{1/2} \tag{7}$$

from the measured values of T_c. The graph of T_c versus p for Equation 5 is drawn in Fig. 11. In this study, the calculated hole carrier concentration decreases from 0.136 to 0.094 with increasing Gd content accompanied by decreasing T_c. In Fig. 12, the calculated values of hole concentrations for our samples using Equations 6 and 7 are plotted. So we get a symmetric curve around the maximum value of T_c. As can be seen from the figure, the relationship between T_c and hole concentration is parabolic for the samples. We observed the dome shaped figure of the T_c vs. hole concentration which is well known for high temperature superconducting cuprates.Thus, the Gd addition reduces the carrier density by affecting the hole concentration. Fig. 13 shows the variation of transition temperature as a function of Gd addition. In Fig. 14, a linear decrease of T_c with Gd addition is clearly seen.

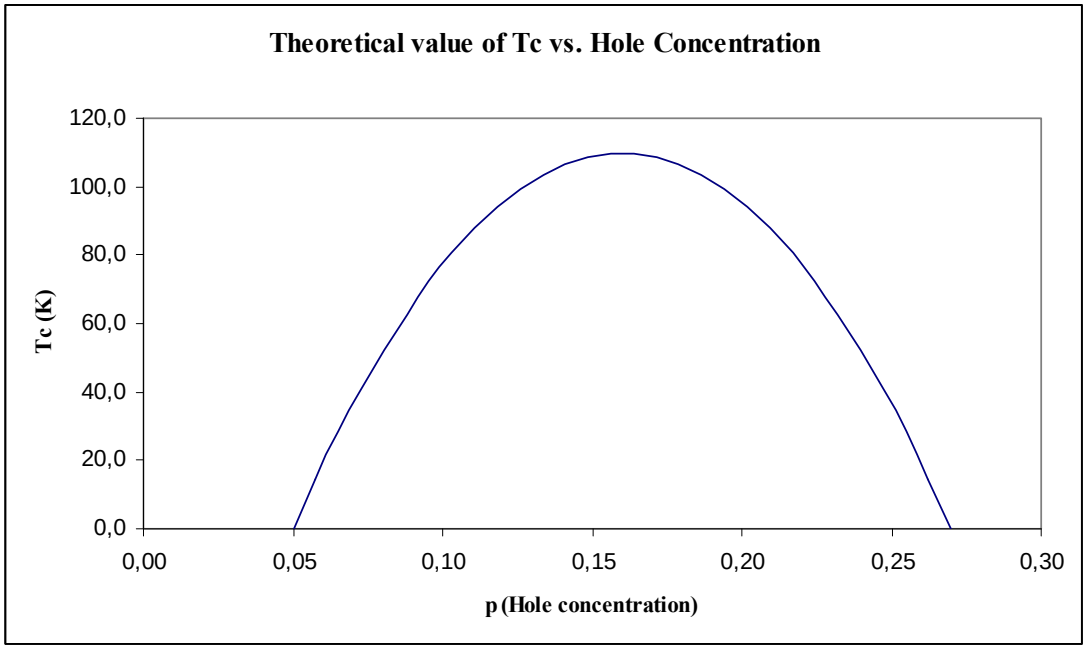

Figure 11. The graph of the Equation 5.

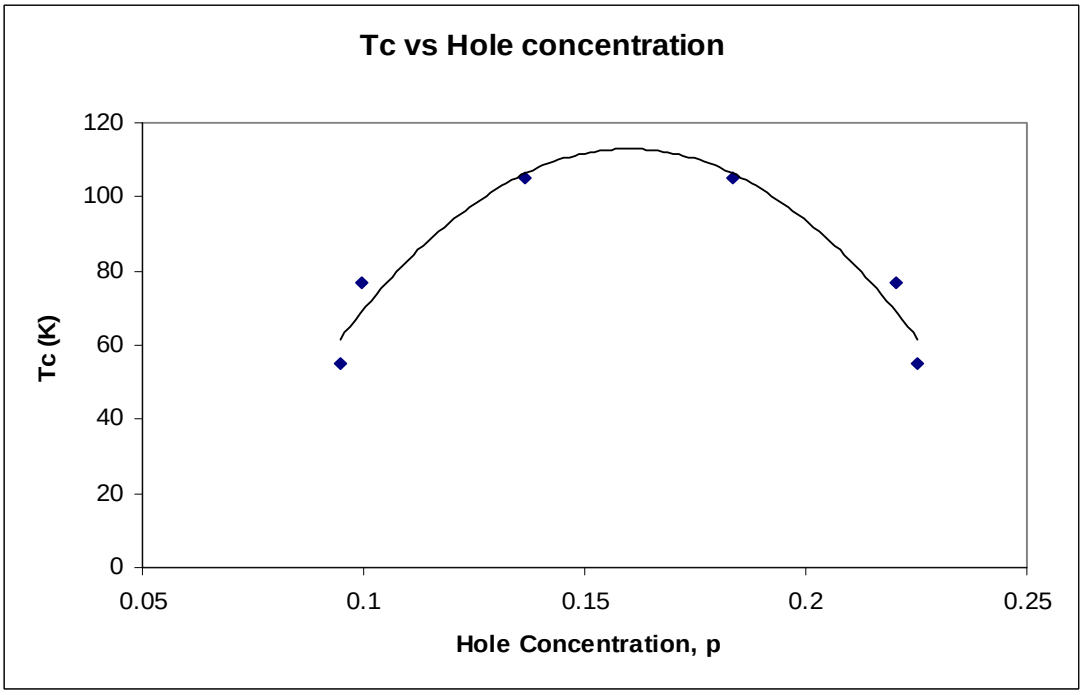

Figure 12. Superconducting transition temperature versus hole concentration of the Gd0, Gd2, Gd4 samples.

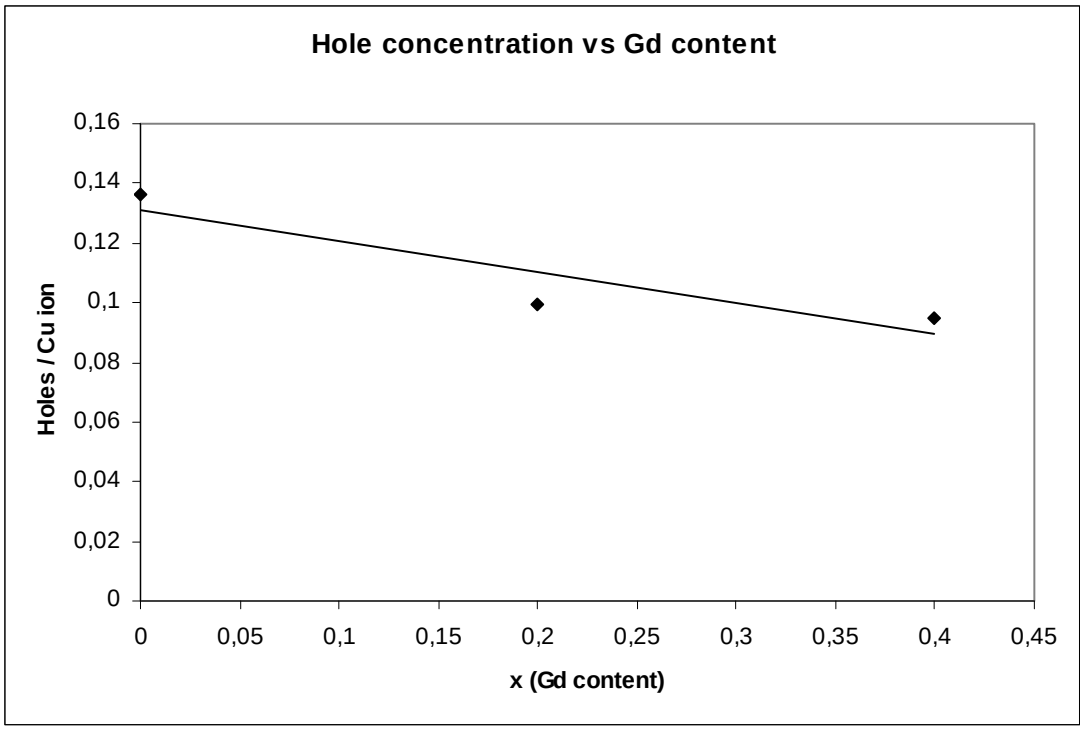

Figure 13. The variation of hole concentration with Gd content

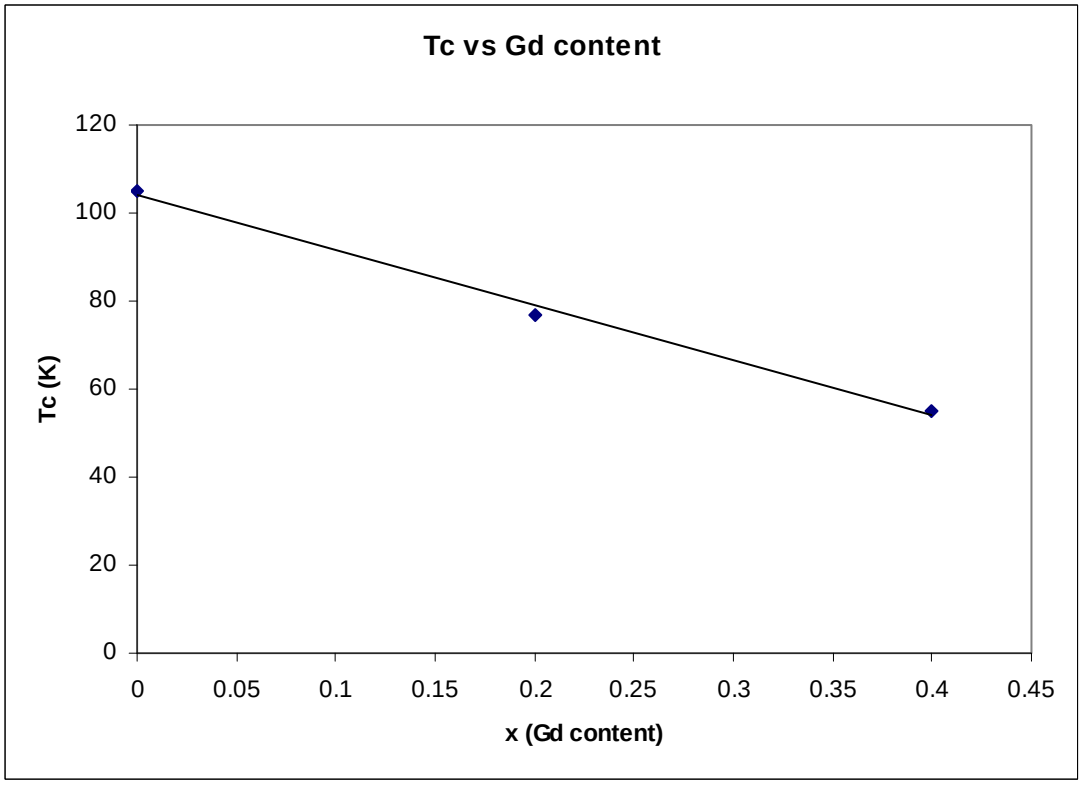

Figure 14. The variation of T_c offset with Gd content.

The high magnetic moment of Gd may also affect the Cooper pairs in the superconducting phase. According to BCS theory, the charge carriers forming the Cooper pairs have opposite spin and momenta. When the pair forms it becomes a bosonic particle. The spins of the pair may have been adversely affected by the magnetic moment of Gd which also resulted in the decrease of carrier concentration by pair-breaking mechanism.

For the critical current density (J_c) measurements, only the samples Gd0 and Gd2 are used since the other sample Gd4 did not show superconducting properties at 77 K. The transport critical current densities of the Gd0 and Gd2 samples measured in liquid nitrogen were 90 and 3 A/cm^2, respectively. It should be noted that the transport critical current density of the Gd added samples is about thirty times less than that of undoped sample. A similar decrease of J_c was observed in Gd-added Bi(Pb)-Sr-Ca-Cu-O [42, 65]. The decrease of J_c in Bi(Pb)-Sr-Ca-Cu-O by Gd addition may be caused by the decrease of grain size, in other words more grain boundaries along the current path and weak links caused by grain boundary regions modified by the presence of Gd atoms. Random orientation of the grains, increased level of impurities and voids may also be partly responsible, although impurities and voids would not have such a big effect on R-T curves. So, it is concluded that main reasons for worsening of the superconducting properties depend strongly on grain boundaries. Gd addition may produce pinning centres in these samples but this improvement is probably less than the observed degrading effect. From the above result, it was inferred that the Gd addition has the negative effect on the J_c and T_c values of the samples [64].

In sample Gd4, which only has 2212 phase, average grain size is further

decreased, causing larger percentage of grain boundary regions. Presence of Gd ions has inhibited grain growth resulting in smaller grains and lower superconducting volume. This is clearly seen as an increased room temperature resistivity (Table 4). The decrease of onset critical temperature with increasing Gd addition shows that Gd ions also substituted Ca ions inside the superconducting grains of both 2223 and 2212 phases [64].

XRD measurements provide data about lattice parameters for Gd added Bi-2223 bulk samples. Room temperature XRD patterns from the surface of the Gd0, Gd2, and Gd4 samples are shown in Fig. 15. L, H, and C in this figure indicate the low-T_c, high-T_c and Ca_2PbO_4 phase, respectively. Phase purity and the lattice parameters were determined from these XRD results. The accuracy in determining the lattice parameters *a* and *c* was ± 0.001 Å. The values of grain sizes can be estimated from XRD measurements by using Scherrer-Warren formula [66],

$$D = \left(0.94\lambda / B\cos\theta\right) \tag{8}$$

where *D* is the crystallite size in nm, λ (15.418 nm) is the wavelength of x-ray in nm, θ is the angle of intensity peak and *B* is the full width at half maximum (FWHM) of the same intensity peak.

With increasing Gd additions, the intensity of the XRD peaks decreases while their positions shift towards larger angles. This phenomenon indicates that average crystallite size becomes smaller as confirmed by SEM investigations. The grain sizes calculated from XRD patterns using Equation 8 are 212, 142, and 112 nm for Gd0, Gd2, and Gd4 samples, respectively.

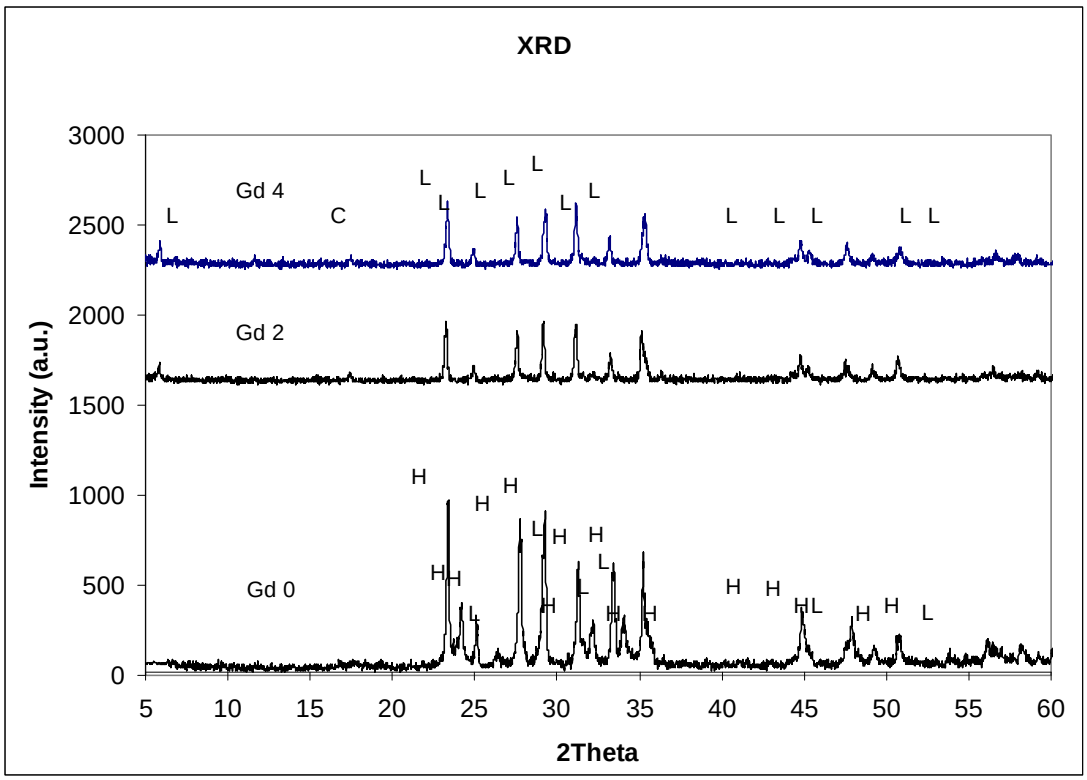

Figure 15. XRD results of the Gd0, Gd2, and Gd4 samples.

The relative volume fractions of the Bi-2223 and Bi-2212 phases in all the samples were estimated from the peak heights of the reflections belonging the same particular crystallographic plane, using the following well-known expressions [67,68];

$$f_{(2223)} = \frac{\sum I_{H(hkl)}}{\sum I_{H(hkl)} + \sum I_{L(hkl)}} \tag{9}$$

$$f_{(2212)} = \frac{\sum I_{L(hkl)}}{\sum I_{H(hkl)} + \sum I_{L(hkl)}} \tag{10}$$

Here $I_{H(hkl)}$ and $I_{L(hkl)}$ are the intensities of the (hkl) diffraction lines for Bi-2223 and Bi-2212 phases, respectively.

It was obtained that the intensities of the peaks corresponding to the Bi-2223 phase decrease and the intensities of the peaks corresponding to the Bi-2212 phase increase with increasing Gd addition. When the Gd content was $x \geq 0.4$, the high-T_c phase reflections were completely absent and only those belonging to the low-T_c and Ca_2PbO_4 phase were present. Volume fractions of the samples calculated using Eqns. 9 and 10 are summarized in Table 4. As seen in the table, with increasing Gd addition for x = 0.2, the volume fraction of Bi-2223 phase decreased and that of Bi-2212 phase increased. Bi-2223 phase was totally absent for samples with $x \geq 0.4$. This result shows that Gd addition favours the growth of Bi-2212 phase. The addition of the sample by Gd degrades formation of the Bi-2223 phase in comparison with undoped sample. It has been reported in the literature that the substitution of rare earth ions for Ca brings about a transition from the Bi-2223 to the Bi-2212 phase [17, 41].

From the XRD data the cell parameters for orthorhombic structure can be calculated as:

$$\frac{1}{d^2} = \frac{h^2}{a^2} + \frac{k^2}{b^2} + \frac{l^2}{c^2} \qquad (11)$$

where d is the distance between the (hkl) planes and *a,b,c* are cell parameters.

The lattice parameter calculations were performed employing the least squares method and using the data extracted from XRD measurements. A monotonic decrease of the lattice parameter *c* accompanied by a simultaneous but small increase in the lattice parameter *a* was observed with increasing Gd addition as seen Figs. 16, 17, 18, and 19.

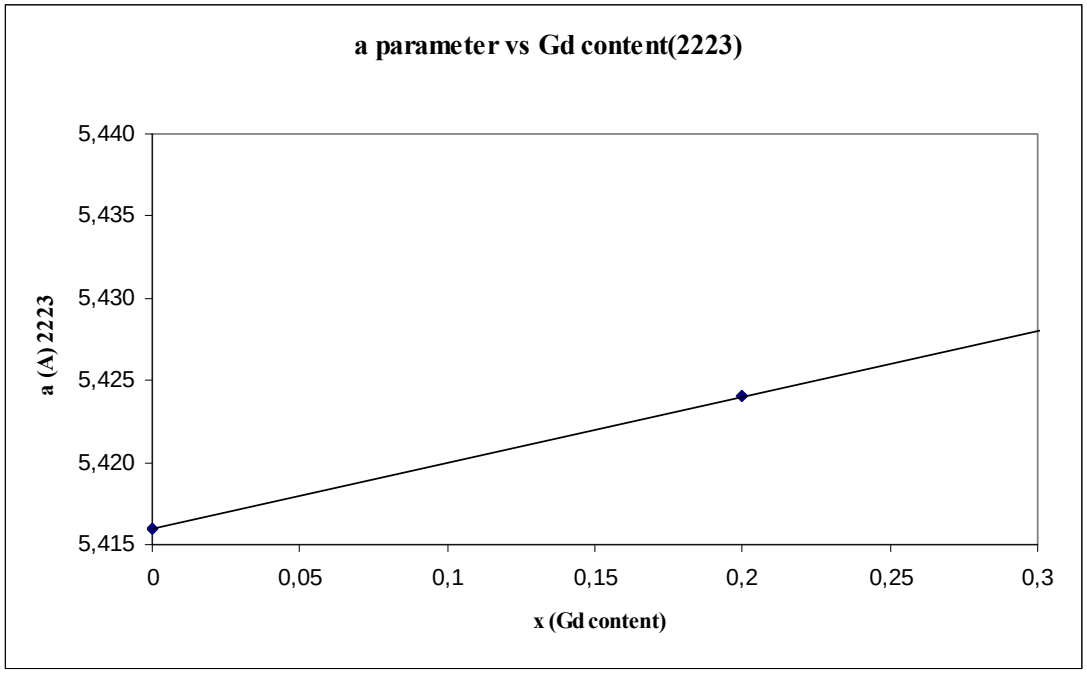

Figure 16. The graph of *a* parameter (2223) vs Gd content.

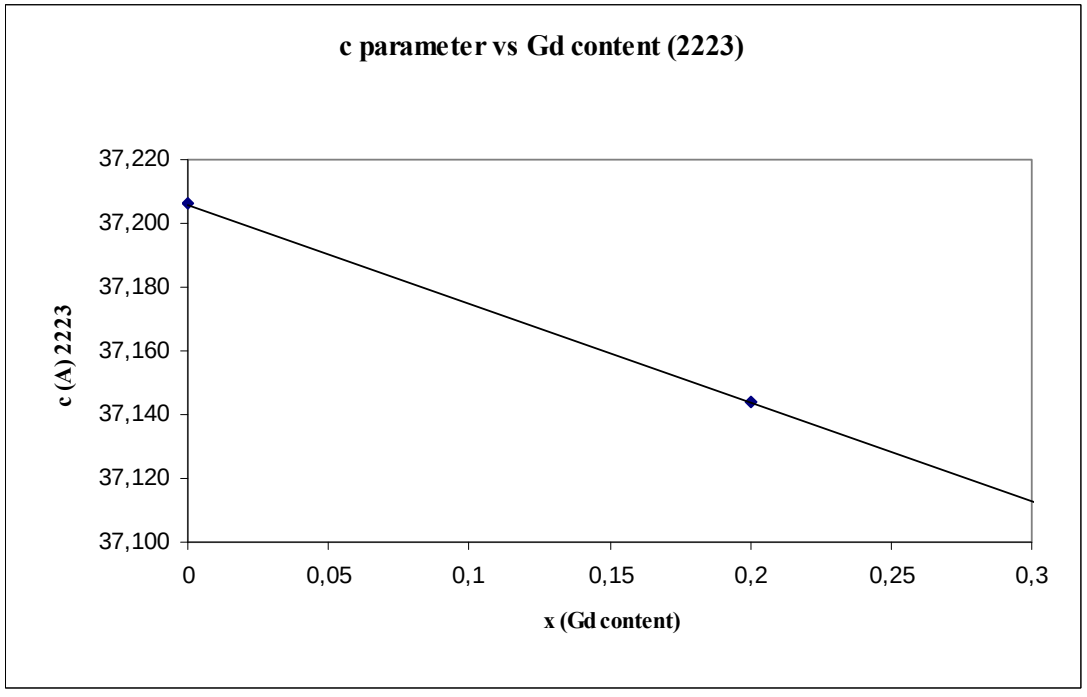

Figure 17. The graph of *c* parameter (2223) vs Gd content

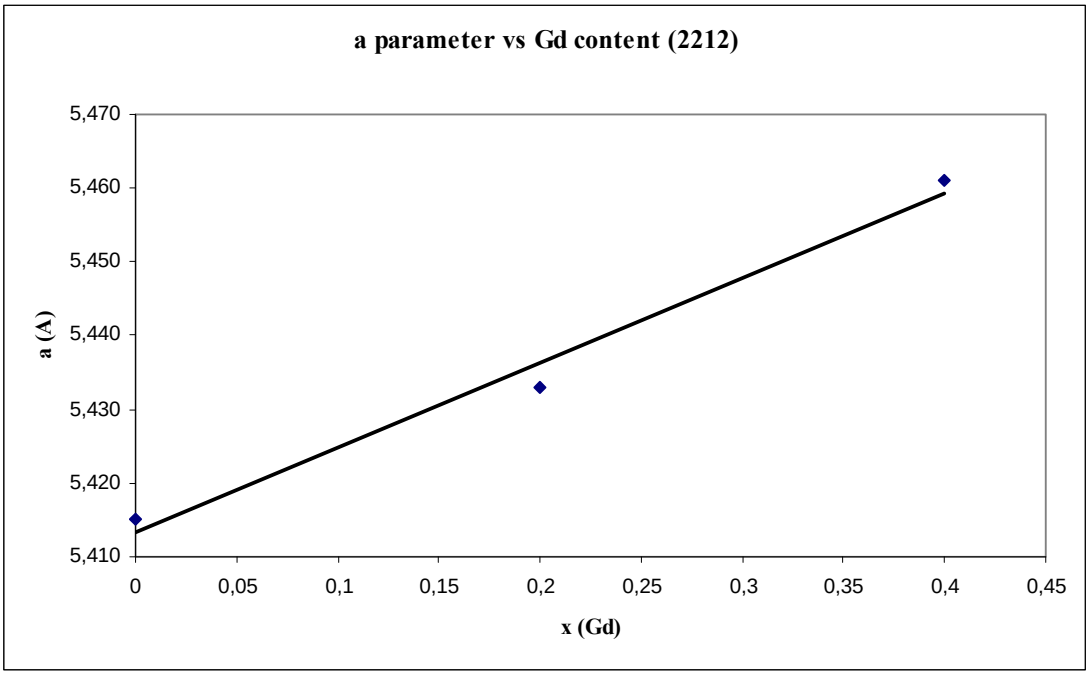

Figure 18. The graph of *a* parameter (2212) vs Gd content

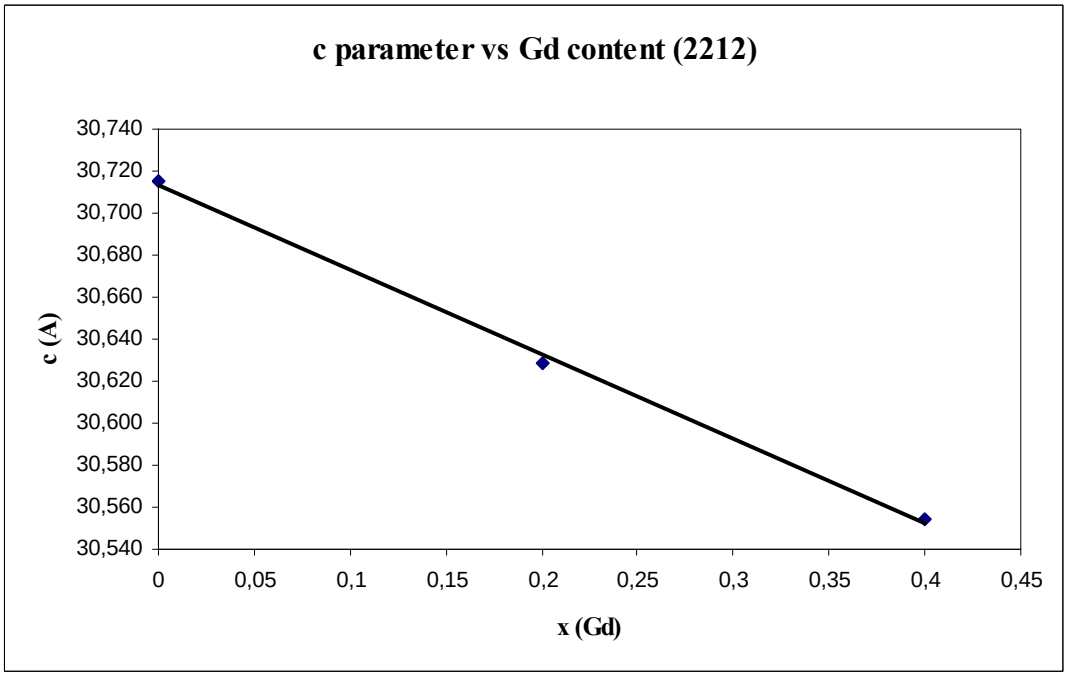

Figure 19. The graph of *c* parameter (2212) vs Gd content

The decrease of *c*-axis length with increasing Gd content may be due to the smaller size of the Gd^{3+} ion compared to the Ca^{2+} ion. However, it is very difficult to understand the increase in the *a* parameter from the substitutional point of view since the *a*-axis length is controlled by the in-plane Cu-O bond distance. The increase in *a* may be due to the decrease of hole concentration that weakens the Cu-O bonding. As the carrier concentration decreases, the number of Cu^{3+} ions, which form a shorter Cu-O bond length compared to the Cu^{2+} ions, decreases. A similar variation in the *a* and *c* parameters has also been observed in the La system when the La^{3+} ion is replaced by a slightly larger Sr^{2+} ions [69].

When the Gd-added samples (Gd2, and Gd4) are compared with the undoped sample (Gd0), a smaller lattice parameter *c*, lower intensity of the XRD peaks and lower volume fraction of the high-T_c phase to the low-T_c phase or nonexistence of high-T_c phase are revealed. This finding is in agreement with some previous works [35, 42, 70].

Cation	Ca^{2+}	Gd^{3+}	Sr^{2+}	Bi^{3+}	Sm^{3+}	Pb^{2+}
Ionic radius(Å)	0.99	0.97	1.12	0.96	0.96	1,20

Table 4. The ionic radii of some cations.

Comparing the ionic radius of Gd^{3+} (0.97 Å) with those of Ca^{2+} (0.99 Å), Sr^{2+} (1.12 Å) and Bi^{3+} (0.96 Å), Gd^{3+} ions can replace any of the above. But Bi^{3+} replacement by Gd^{3+} would not produce a drastic change in the superconducting properties. Because the valencies of both ions are the same so the hole density does not change, and their sizes are nearly the same [64].

The surface morphology of the Gd added Bi(Pb)-Sr-Ca-Cu-O samples was studied by SEM. Fig. 20 represents surface micrographs for the Gd0, Gd2, and Gd4 samples. The microstructure of Gd0 sample is remarkably different from that of Gd2, and Gd4 samples. A broad grain size distribution can be seen for the Gd0 sample. The grain sizes are seen to decrease with Gd addition from SEM graphs. This is also in aggrement with the calculated values of grain sizes from XRD peaks. It is observed that the grain connectivity is worsened greatly with increasing Gd addition. The surface of the Gd0 sample is more uniform with better alignment of grains. SEM photographs of Gd0 shows better crystallinity in comparison with the remaining samples. Gd4 has the worst appearance among these four samples. There are voids, porosities and signs of partial melting on the micrograph of Gd4. This shows that as the Gd content increases the melting temperature of the samples decrease.

These results indicate that the surface morphology of the sample is worsened with increasing Gd addition. Melting and solidification process may be responsible for the worsening of the microstructure.

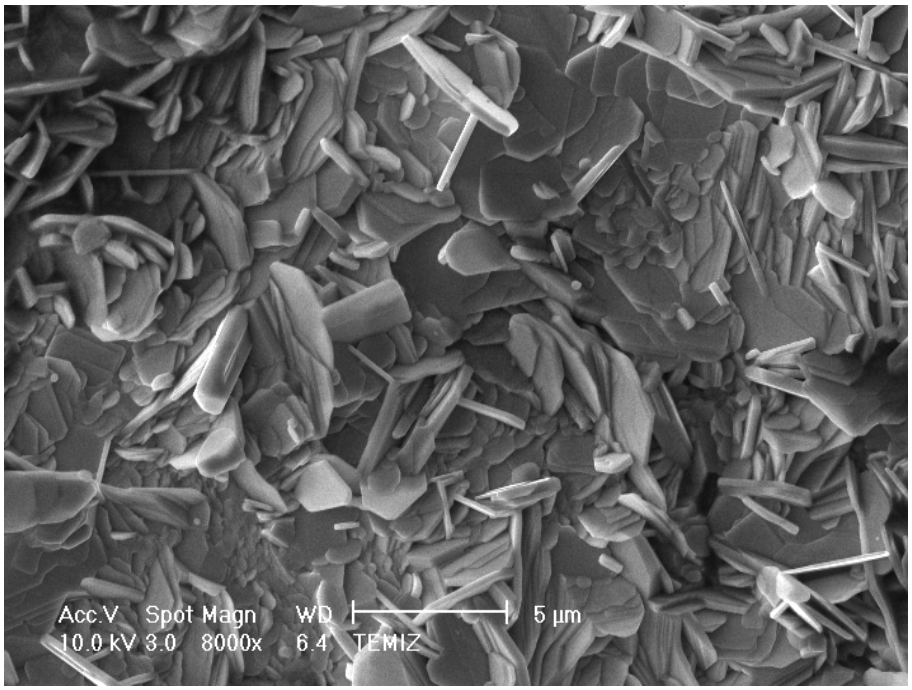
Acc.V Spot Magn WD 5 µm
10.0 kV 3.0 8000x 6.4 TEMIZ

(a)

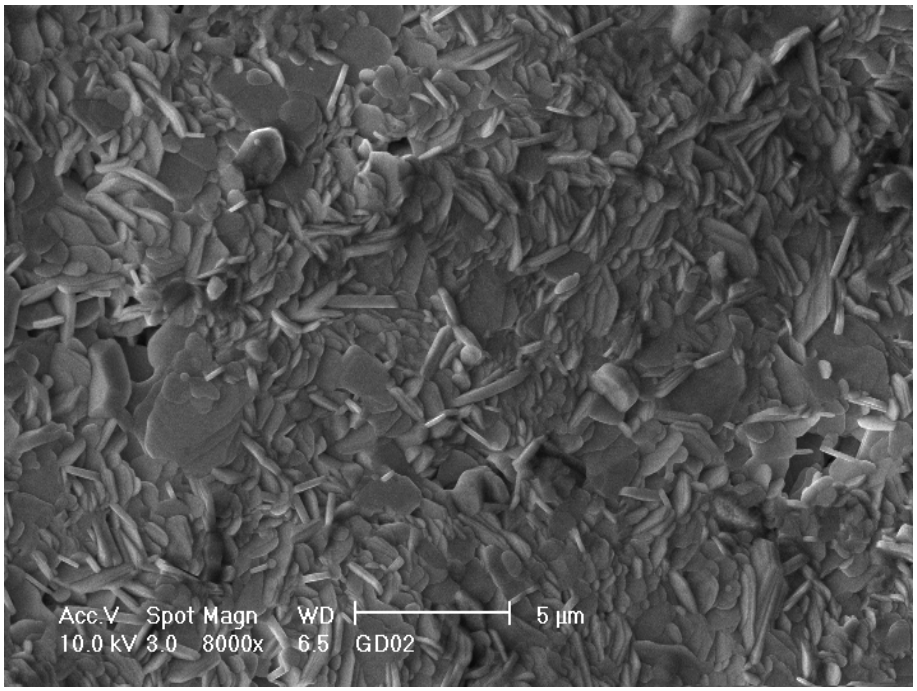
Acc.V Spot Magn WD 5 µm
10.0 kV 3.0 8000x 6.5 GD02

(b)

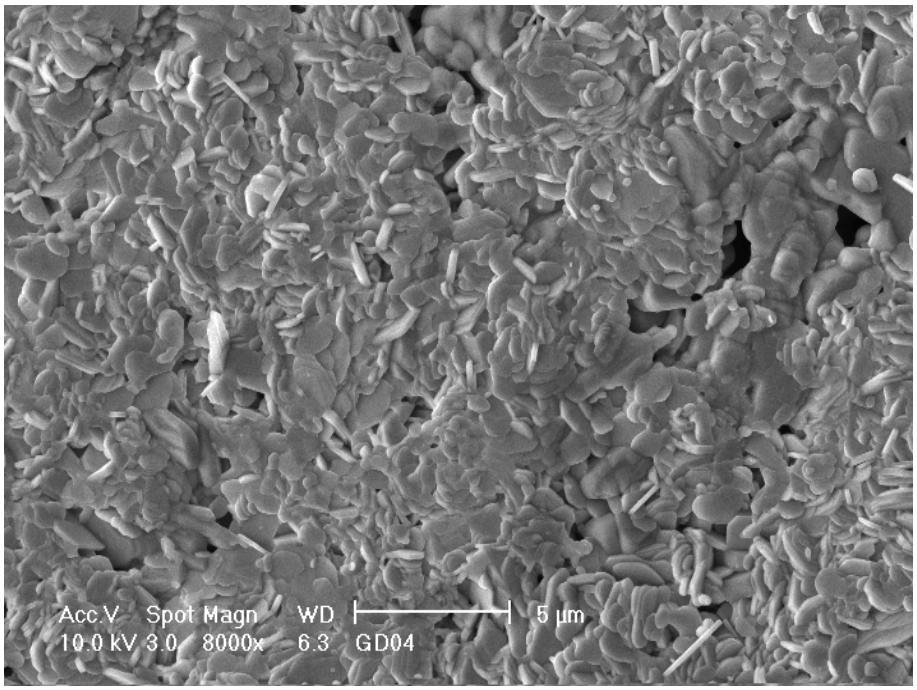

(c)

Figure 20. SEM micrographs of the (a) Gd0 (b) Gd2 and (c) Gd4 samples.

To investigate the effect of Gd addition on the mechanical properties of the samples, we measured the diagonal length as a function of test load. Conventional Vickers microhardness measurements consist of applying a load F on the test material via a geometrically defined indenter and after the indenter is removed, measuring the characteristic dimension *d* of the resultant impression.

In Fig. 21 below, typical indentation for an applied load of 1.96 N for Gd4 sample is shown.

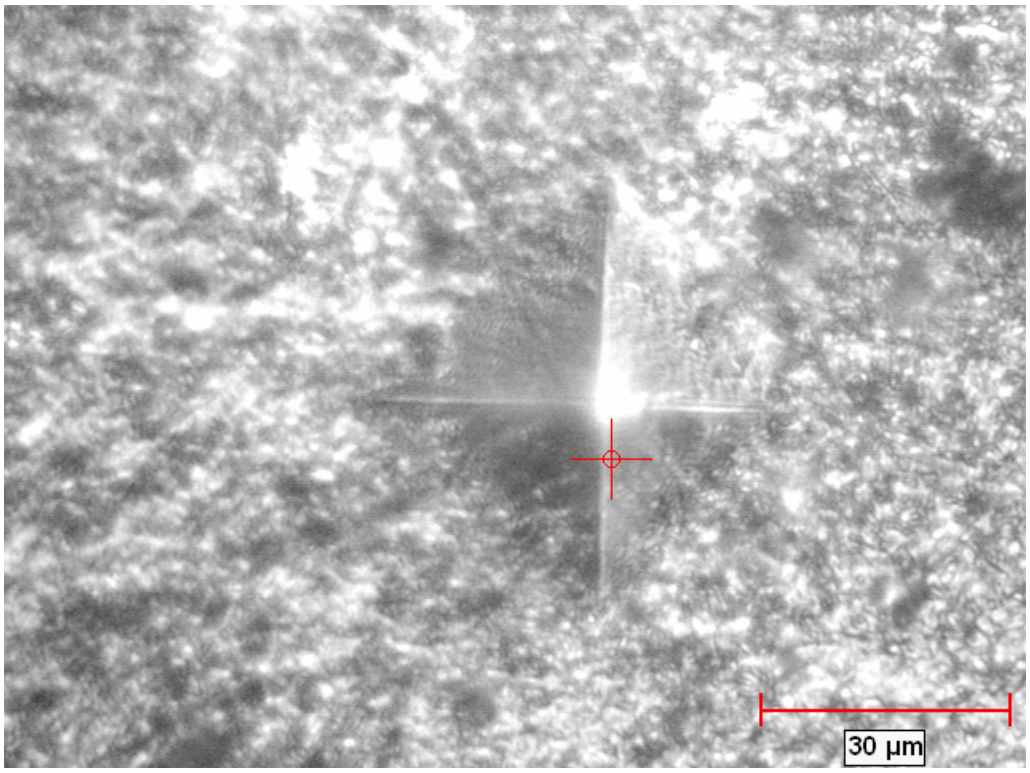

Figure 21. Typical indentation for an applied load of 1.96 N for Gd4 sample.

The Vickers microhardness (apparent) values of different applied loads were calculated by using the equation from Ref. [71],

$$H_v = 1854.4\left(F/d^2\right) \qquad (GPa) \tag{12}$$

where F is the applied load in N and d is the diagonal length of the indentation mark in µm.

In most materials, the elastic modulus (Young's modulus), E, is related to the Vickers microhardness (apparent) H_v by the relation [72]

$$E = 81.9635 H_v \tag{13}$$

and yield strength Y is related to the hardness by the relation [73,74]

$$Y \approx H_v/3. \tag{14}$$

It is useful to mention the fracture toughness, K_{IC}, as it is one of the main mechanical properties of superconducting samples. The fracture toughness is an important parameter for the selection of materials for applications. Due to the nature of intrinsic brittleness, microindentation may result in microfracture around the impressed region on the surface of the samples [75]. Since microfracture occurs mainly during the loading a portion of the energy, which is used to create the indentation deformation, will be dissipated by the crack formation. Owing to the definition of the K_{IC} as the critical stress intensity factor, it is directly related to γ of the crack faces [76]

$$K_{IC} = \sqrt{2E\gamma}. \tag{15}$$

Fig. 22 displays the variation of microhardness as a function of the applied load for the Gd0, Gd2, and Gd4 samples. The variation of microhardness with load has similar shape irrespective of the amount of Gd addition although numerical values are different. We have observed that the microhardness values decrease with increase in Gd addition.

The calculated load dependent microhardness, Young's Modulus, yield strength, and fracture toughness values at 2.94 N load using Eq. (12-15) were summarized in Table 5. The values of H_v at 2.94 N for Gd0, Gd2, and Gd4 samples are 0.534, 0.261, and 0.230 GPa respectively. This decrease is attributed to the formation of impurity phases and irregularities mainly distributed at the grain

boundaries. These impurities and irregularities cause distortion of the bond strength, and consequently the hardness values decrease [64,77].

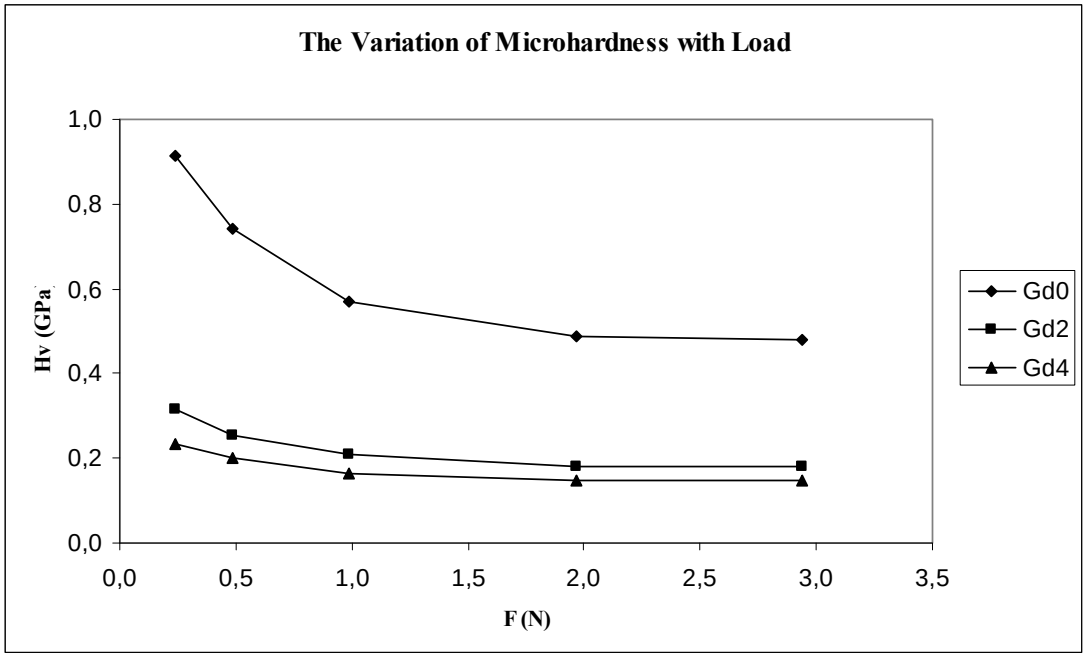

Figure 22. The Variation of Microhardness with Load.

Samples	$H_v(GPa)$ at 2.94 N	$E(GPa)$ At 2.94 N	$Y(GPa)$ at 2.94 N	$K_{IC}(Pa/\sqrt{m})$ at 2.94 N
Gd0	0.534	43.8	0.178	22.89
Gd2	0.261	21.4	0.087	14.87
Gd4	0.230	18.8	0.076	11.34

Table 5. The load dependent values of H_v, E, Y, and K_{IC} corresponding to each sample calculated at 2.94 N.

This similar change in H_v with increase in Gd addition is also revealed for the critical transition temperature in our measurements. It was observed that Vickers hardness decreased with increasing amount of doping and addition in Bi-2223 superconductors [37]. Rapid variation of microhardness was observed with increasing applied load from 0.245 to 0.980 N. The reason for this behaviour may be due to the contribution of weak grain boundaries [78]. It is also obvious from the figure that the Vickers microhardness values are load dependent for all samples; the calculated microhardness value decreases non-linearly as the applied load decreased until 0.980 N, then it tends to attain saturation. As reported by Khalil [79], this behavior can be explained as following;

a) at larger indention loads, the Vickers hardness registered smaller values, this observation may be due to the presence of weak grain boundaries of the superconducting ceramics;

b) at smaller indention loads, the Vickers hardness recorded higher values, these measured hardness values may be more indicative of the monocrystalline state without interference from grain boundaries.

This non-linear behavior has also been observed in the literature for Bi-Pb-Sr-Ca-Cu-O samples [80,81] and is known as indentation size effect (ISE) [77,82,83].

The variation of H_v of the samples is plotted as a function of Gd content in Fig. 23. As seen in this graph, the load dependent H_v decrease with a rise in the Gd addition. Since E, Y and K_{IC} values are directly proportional to H_v mathematically apart from some constants, thus E, Y and K_{IC} have the same behaviour. This behavior is due to crack initiation and degradation of microhardness. This indicates

that the Gd addition softens the superconductor materials further with higher amounts. When Gd is partially substituted by Ca, interplayer bonding is weakened as confirmed by the decrease in H_v, E, Y and K_{IC} values. A decrease in K_{IC} corresponds to a decrease in the average surface energy as proposed from the hardness calculations. One should point out that the apparent microhardness; Young's modulus, yield strength, and fracture toughness of the samples in the present work indicate strong dependency on applied load.

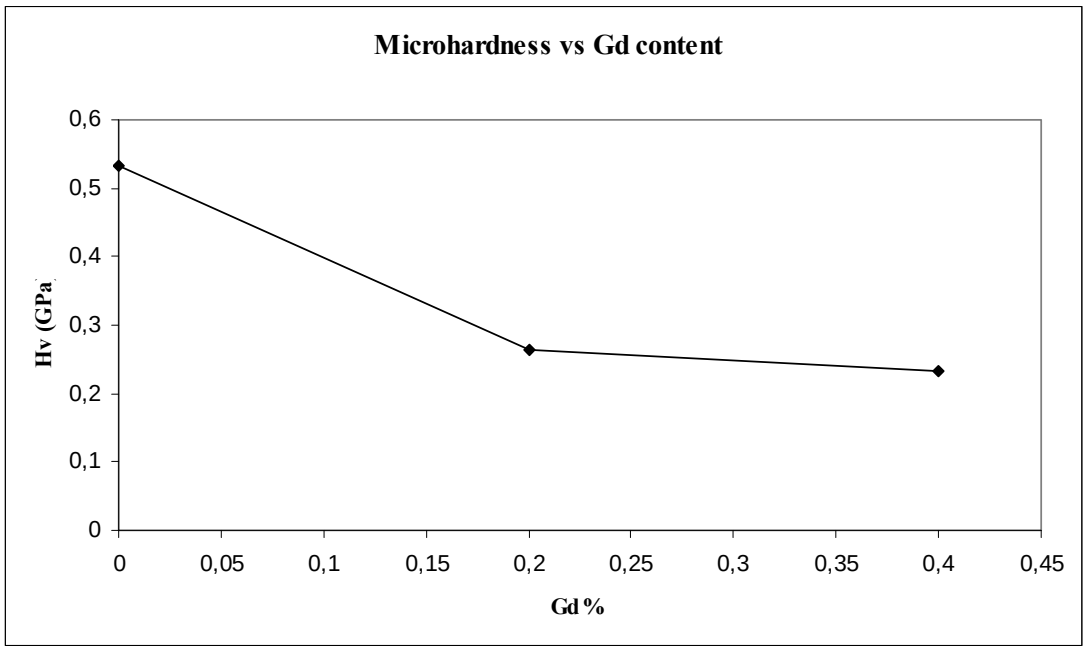

Figure 23. The variation of load dependent Vickers microhardness of the samples as a function of Gd content.

To account for this effect, several relationships between the applied load and the resulting indentation size have been suggested [84,85,86]. This effect can be explained by two different methods [70]. The first method assumes that the indentation contains an elastic portion. The elastic part of the deformation is relaxed

upon loading. This can be accounted for by adding an elastic component, d_e, to the measured plastic indentation semidiagonal, d_p. Thus, a true hardness, H_0, is defined from

$$H_0 = 1854.4\left(\frac{F}{(d_p + d_e)^2}\right) \qquad (GPa) \qquad (16)$$

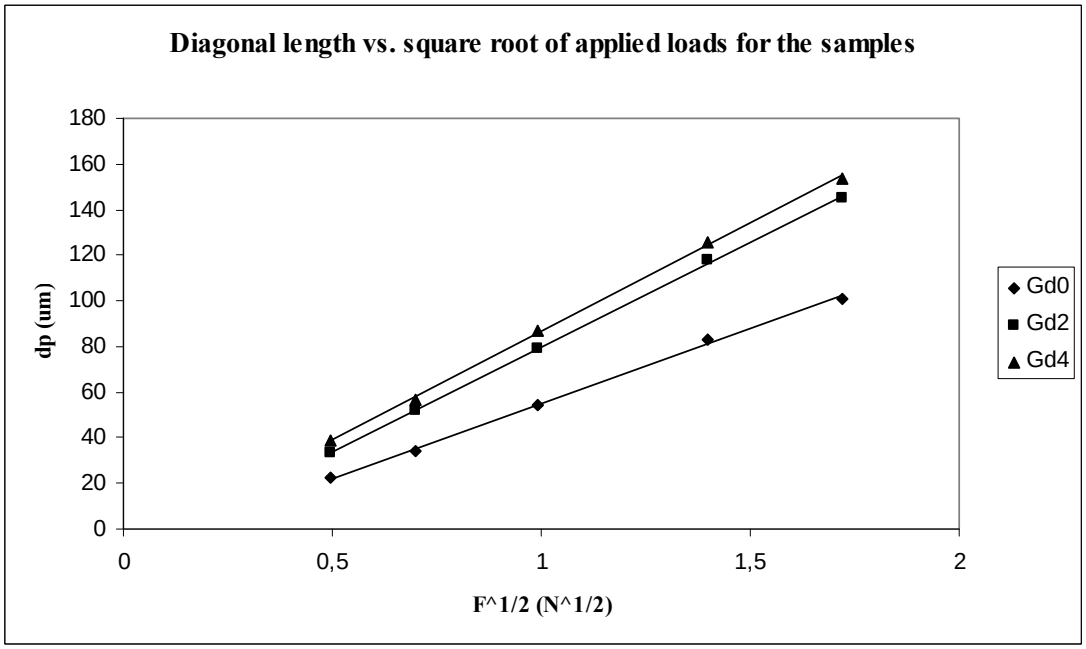

Figure 24. Plots of diagonal length versus square root of applied loads for the samples.

Fig. 24 exhibits d_p versus $F^{1/2}$ plots for Gd0, Gd2, and Gd4 samples. Therefore, Eq. 16 indicates that measured indentation diagonals should be linear with the square root of the applied load and the slope of such a curve is proportional to $1/(H_0)^{1/2}$ and the vertical intercept of this graph is proportional to the elastic part of the indentation semi diagonal, d_e. The extracted values of H_o, d_e and LRC are listed in Table 6.

Samples	H_0 *(GPa)*	d_e (μm)	*LRC*	H_V *(GPa) in plateau region*
Gd0	0.432	10.6	0.99971	0.534-0.538
Gd2	0.224	10.9	0.99987	0.261-0.262
Gd4	0.204	8.57	0.99989	0.229-0.230

Table 6. Best-fit results of experimental data according to Eq. 16.

It was obvious that such plots are linear with the estimated linear regression coefficients (LRC) always better than 99.9%, implying that Eq. 16 provides a satisfactory description to calculate the true hardness of the indentation data for the samples. As can be seen from the table, the increase in Gd addition decreased the values of H_o but d_e of the samples changes randomly. Quin et al. [87] investigated the variation of Vickers microhardness as a function of indentation load for a variety of ceramic materials. They observed that such hardness-load curve shows distinct transition to a plateau of the constant hardness level and concluded that the transition in such curves correspond to the intrinsic hardness value of the material. In this study, this plateau is reached at 1.96 N applied load for the samples. As can be seen from Table 6, true microhardness value of Gd0 sample (0.432 GPa) is lower than the hardness results in the plateau region (saturated region) (H_v = 0.534 GPa). This behavior is also observed in other samples (Gd2, and Gd4) in this work. This result revealed that the true hardness of the sample is lower than that of the traditionally calculated ones. The calculations of H_0 values for the investigated samples also indicated that the magnitude of d_e to be 10.6 for Gd0, and 10.9 and 8.57 μm for Gd

added samples (Gd2, and Gd4). These extracted magnitudes of d_e infer that the amount of relaxation of diagonal length is significant with respect to the measured diagonals at low indentation loads and hence the ISE is pronounced for the low load range.

The second method considers energy dissipative processes during the indentation rather than elastic processes. In this model, a true microhardness can be defined by subtracting a dissipative part, F_0, from the applied load [70]

$$H_0 = 1854.4\left(\frac{F - F_0}{d^2}\right) \qquad (GPa) \tag{17}$$

Fig. 25 exhibits applied load as a function of the square of the diagonal length for the samples. Each set of data shows linear relationship. The slope of each line corresponds to the load independent hardness constant, H_0 and the intercept of each line represents the sample resistance pressure, F_0. The extracted values of F_0, H_0 and LRC were listed in Table 7.

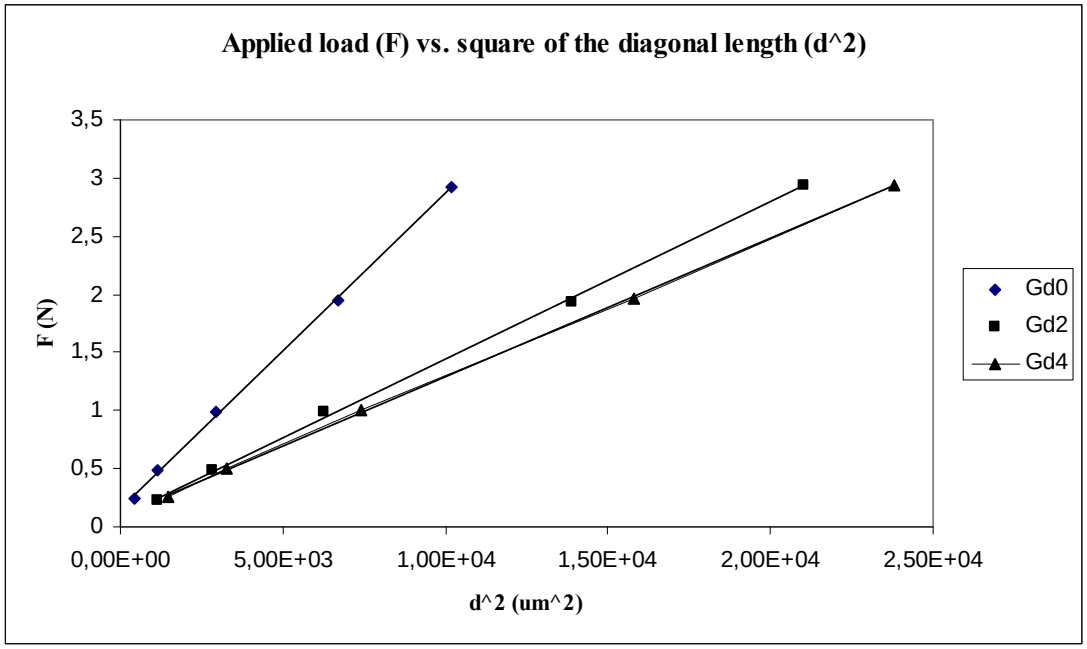

Figure 25. Graph of the applied load against the square of the diagonal length for the samples.

Samples	***H_0 (GPa)***	***F_0 (mN)***	***LRC***	***H_V (GPa) in plateau region***
Gd0	0.507	143	0.99966	0.534-0.538
Gd2	0.251	107	0.99984	0.261-0.262
Gd4	0.223	78.0	0.99992	0.229-0.230

Table 7. Best-fit results of experimental data according to Eq. (17).

As can be seen from this table, the values of F_0 and H_0 of the samples decreased with increasing the Gd addition and the LRC of each sample is very high, implying that Eq. 17 provides a satisfactory description of the indentation data for the samples. It is observed that the estimated true microhardness value of Gd0 sample (0.507 GPa) using the second method is lower than the load dependent microhardness

results in the saturated region (H_v = 0.534 GPa). But this discrepancy between the load dependent and independent microhardness values using the second method is smaller than that of the first method. We can conclude that the second method is more convenient than the first method for our experimental data.

On the other hand, it is observed that the diagonal length is strongly dependent on the applied load from the experimental observations. This observation is governed by [37].

$$\frac{F}{d} = H_0 d + \gamma \tag{18}$$

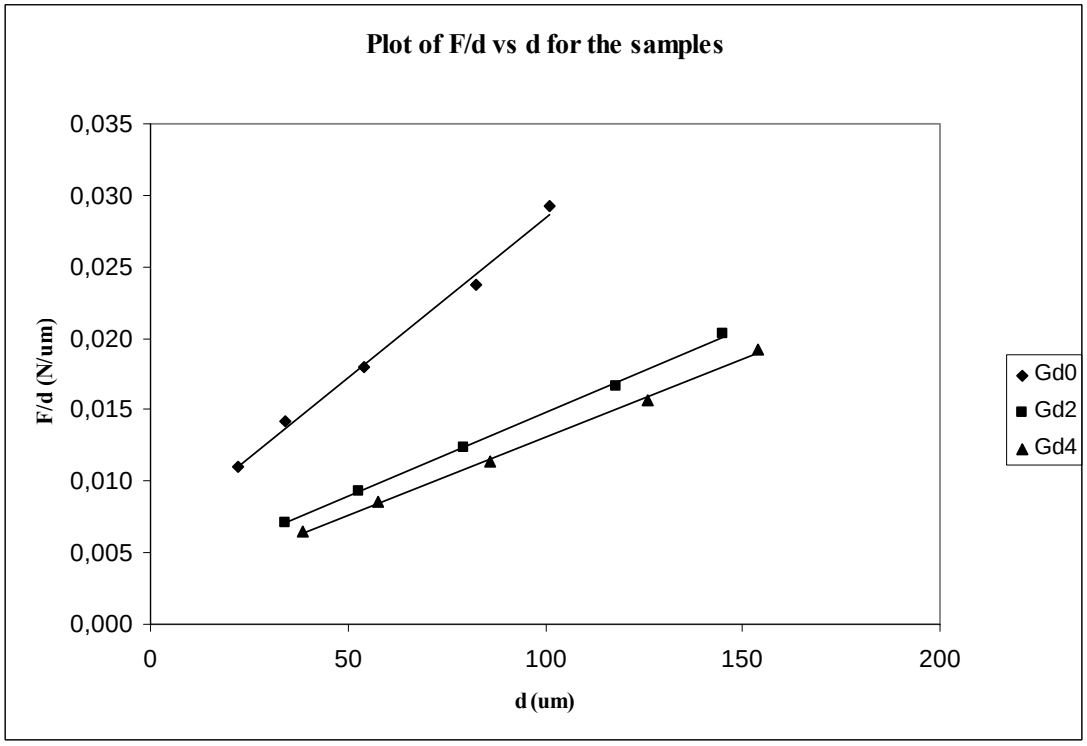

Figure 26. Plots of F/d versus d for the samples.

Fig. 26 exhibits the values of F/d against the diagonal length of indentation, d, for the samples. Each set of data shows linear relationship. The slope of each line corresponds to the true hardness, H_0 and the intercept of each line represents the surface energy γ. The extracted values of H_0, γ and LRC were listed in Table 8.

Samples	***H_0 (GPa)***	***γ x10^{-3} (N/μm)***	***LRC***
Gd0	0.519	6.16	0.9990
Gd2	0.438	3.08	0.9990
Gd4	0.368	2.13	0.9991

Table 8. Best-fit results of experimental data according to Eq. 18.

It was observed that the values of H_0 and γ of the all samples decreased with increasing the Gd addition. This observation is ascribed to the dissipation of the energy of cracks at the interfaces [70].

One can calculate E, Y, and K_{IC} using true microhardness (load independent, H_0) calculated by Eq. 18 for each sample. The variations of load independent H_0, as a function of Gd addition are plotted in Fig. 27.

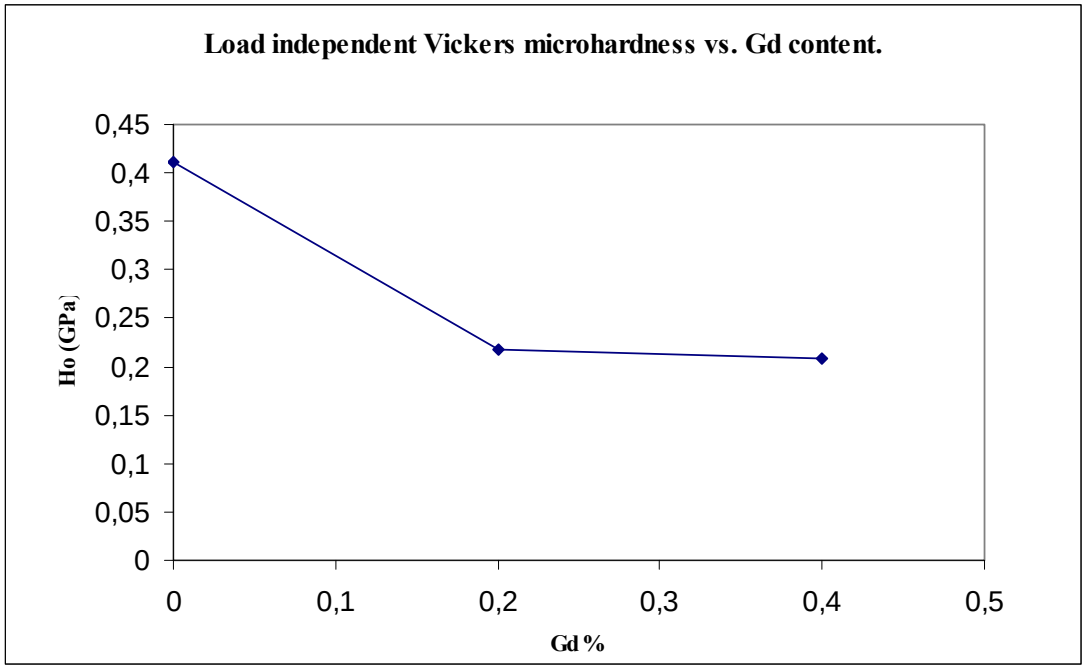

Figure 27. The variations of load independent Vickers microhardness of the samples as a function of Gd content.

Since E_0, Y_0, K_{IC0} values are directly proportional to H_0 mathematically apart from some constants, E, Y and K_{IC} have the same behaviour. From the figure, it is clear that the load independent values of E_0, Y_0, K_{IC0} decrease significantly with increasing the Gd addition. Comparing Figs. 23 and 27, it is concluded that the load independent values are lower than that of load dependent values. This is in agreement with the literature [70,88]. The above results revealed that by increasing the Gd addition, it is possible to control the mechanical properties of the samples. Gd addition has negative effect on mechanical properties of BSCCO system.

CHAPTER 6

CONCLUSION

In this work the effect of Gd addition into the BSCCO 2223 system is studied. The superconducting properties of the system were deteriorated as the amount of Gd increased.

The addition of Gd degraded the formation of the 2223 phase and hence as the Gd content increased the volume fraction of 2223 phase decreased while that of 2212 increased.

Zero-resistivity transition temperatures of the Gd0, Gd2, Gd4 samples are determined as 105 K, 77 K, and 55 K, respectively. The T_c values decreased with increasing Gd addition.

The hole concentration decreased with the addition of Gd. This resulted in a decrease of T_c values.

The transport critical current density decreased with increasing Gd content. The J_c values for Gd0, and Gd2 samples are determined as 90 A/cm^2 and 3 A/cm^2. For the Gd4 sample, the superconductivity was not observed at 77 K.

There is broadening of transition and the connection between the grains also degraded by the addition of Gd. Weak links and impurities increase with increasing

Gd content.

The *c* parameter of the unit cell decreases with increasing Gd content while the a parameter increases slightly.

To better understand whether the dominant reason for the changes on the superconducting properties upon doping by rare earths is due to magnetic effects or due to the change in hole concentration, more future work and results are needed.

The microstructure degrades as the Gd content increases. Grain sizes decrease and the alingment of the grains is weakened. Also as the Gd content increased to x=0.4 porosities in the structure are evident. Occurance of pores is a clue for the worse connection between grains. The density of the microstructure decreases with Gd addition. There is also partial melting for the sample with high concentration of Gd. The contact area among the grains decreases with Gd addition.

The mechanical properties degrade also with the addition of Gd. This is due to the increase in voids, impurity phase, and resistance to crack propagation.

The estimated apparent microhardness, Young's modulus, yield strength and fracture toughness values of the samples depend on applied load and Gd addition. They decrease with the increase in the load and Gd addition.

The ISE behaviour can be examined two different methods. The first method suggests that the indentation contains an elastic portion. The elastic part of the deformation is relaxed upon loading. The second method considers energy dissipative processes during the indentation rather than elastic processes. In this model, a true microhardness can be defined by subtracting a dissipative part, F_0, from

the applied load. In our study, the second model is found to be more convenient for describing the experimental data.

REFERENCES

[1] T. P. Sheanen, *Introduction to High Temperature Superconductivity*, Kluwer Academic Pub. (2002)

[2] H. K. Onnes, *The resistance of pure mercury at helium temperatures*, Commun. Phys. Lab. Univ. Leiden **12**, 120 (1911).

[3] W. *Meissner and R. Ochsenfeld*, *Ein neuer Effekt bei Eintritt der Supraleitfähigkeit*, Naturwissenschaften, **21,** 787–788 (1933).

[4] J. Bardeen, L. N. Cooper, and J. R. Schrieffer, *Theory of Superconductivity*, Phys. Rev. **108,** 1175–1205 (1957).

[5] J. G. Bednorz and K.A. Mueller, *Possible high T_C superconductivity in the Ba-La-Cu-O system*, Z. Phys. **B64,** 189–193 (1986).

[6] M. K. Wu, J. R. Ashburn, C. J. Torng, P. H. Hor, R. L. Meng, L. Gao, Z. J. Huang, Y. Q. Wang, and C. W. Chu, *Superconductivity at 93 K in a New Mixed- Phase Y-Ba-Cu-O Compound System at Ambient Pressure*, Phys. Rev. Lett. **58**, 908-910 (1987)

[7] H. Maeda, Y. Tanaka, M. Fukutomi, T. Asano, *A New High-T_c Oxide Superconductor without a Rare Earth Element*, Jpn. J. Appl. Phys., **27**, L209 (1988).

[8] H. L. Luo and Yu Mei , *Thin Films of the High-T_c Bi-Sr-Ca-Cu Oxide System - A Brief Review*, Chin. J of Phys. **28**, No. 5 (1990)

[9] M.R. Presland, J. L. Tallon, R. G. Buckley, R. S. Liu, N. E. Floer, *General trends in oxygen stoichiometry effects on T_c in Bi and Tl superconductors* ,Physica C **176,** 95 (1991)

[10] S. Nhien and G. Desgardin, *Synthesis and reaction mechanism of the high-T_c 2223 phase in the (Bi,Pb)-Sr-Ca-Ca-Cu-O system*, Physica C **272**, 309 (1996)

[11] İ. Belenli , Investigation Of Processing Routes For The Production Of Wires And Tapes From Bismuth-Based High Temperature Superconducting (HTS) Ceramic Oxides, PhD Thesis, Pembroke College 1993

[12] L. D. Sýkorová, O. Smrčková, and V. Jakeš , *Effect of doping on properties of Bi-based superconductors*, Phys. Stat. Sol. (c) 1, No. **7**, 1952–1956 (2004)

[13] T. Kawai, T. Horiuchi, K. Mitsui, K. Ogura, S. Takagi, and S. Kawai, *Effect of alkaline metal substitutions to Bi-Sr-Ca-Cu-O superconductor*, Physica C **161**, 561 (1989).

[14] V.V. Petrashko, N.D. Zhigadlo, and Z.A. Semenenko, Technol. Phys. Lett. **22**, 48 (1996)

[15] N. D. Zhigadlo, V. V. Petrashko, Yu. A. Semenenko, C. Panagopoulos, *The effects of Cs doping, heat treatments on the phase formation and superconducting properties of (Bi,Pb)–Sr–Ca–Cu–O ceramics*, Physica C **299**, 327–337 (1998).

[16] A. Jeremie, K. Alami-Yadri, J. C. Grivel and R. Flukiger, *Bi,Pb(2212) and Bi(2223) formation in the Bi-Pb-Sr-Ca-Cu-O system*, Supercond. Sci. Technol. 6, 730-735 (1993)

[17] J. C. Grivel and R. Flukiger, *Formation mechanism of the Pb free $Bi_2Sr_2Ca_2Cu_3O_{10}$ phase*, Supercond. Sci. Technol. **11**, 288–298 (1998)

[18] R. B. Marinenko, and M. Teplitsky, *Quantitative Electron Probe Microanalysis of Bi-Sr-Ca-Cu-O High T_c Superconductors Using Energy- and Wavelength-Dispersive Spectrometry*, Microsc. Microanal. **3**, 504 (1997)

[19] M. Takano, J. Takada, and T. K. Oda, *High-T_c Phase Promoted and Stabilized in the Hi, Pb-Sr-Ca-Cu-O System*, Japan. J. of App. Phys. **27**, L1041-L1043 (1988).

[20] M. M. Ibrahim, S. M. Khalil, and A. M. Ahmed, *Effect of Pb addition on thermoelectric power and microhardness of Bi–Pb–Sr–Ca–Cu–O superconductors*, Journal of Physics and Chemistry of Solids **61**, 1553 (2000).

[21] V. Shelke, H. S. Tewari, N. K. Gaur, R. K. Singh, *Effect of Hg addition on synthesis of Bi-based superconductors*, Physica C **300**, 217 (1998)

[22] J. B. Torrance, A. Bezinge, A. I. Nazzal, T. C. Huang, S. S. P. Parkin, D. T. Keane, S. J. LaPlaca, P. M. Horn, and G. A. Held, *Properties that change as superconductivity disappears at high-doping concentrations in $La_{2-x}Sr_xCuO_4$* , Phys. Rev. B **40**, 8872 (1988)

[23] J. B. Torrance, Y. Tokura, A. I. Nazzal, A. Bezinge, T. C. Huang, and S. S. Parkin, *Anomalous Disappearance of High-Tc Superconductivity at High Hole Concentration in Metallic $La_{2-x}Sr_xCuO_4$*, Phys. Rev. Lett. **61**, 1127 (1988).

[24] Y. Shimakawa, Y. Kubo, T. Manako, and H. Igarashi, *Variation in T_c and carrier concentration in Tl-based superconductors*, Phys. Rev. B **40**,11400 (1989).

[25] A. Matsuda, K. Kinoshita, T. Ishii, H. Shibata, T. Watanabe, and T. Yamada, *Electronic properties of $Ba_2Y_{1-x}Pr_xCu_3O_{7-\delta}$*, Phys. Rev. B **38**, 2910 (1988).

[26] Z. Z. Wang, J. Clayhold, N. P. Ong, J. M. Tarascon, L. H. Greene, W. R. McKinnon, and G. W. Hull, *Variation of superconductivity with carrier concentration in oxygen-doped* $YBa_2Cu_3O_{7-y}$, Phys. Rev. B **36**, 7222 (1987)

[27] M. Rateau, R. Suryanarayanan, O. Gorochov, and H. Pankowska, *Carrier-density-related superconductivity in bismuth cuprates*, Phys. Rev. B **41**, 857 (1990)

[28] K. Oto, K. Murase and S. Takaoka, Resistivity, *Hall coefficient and transition temperatures in doped 80K and 110K Bi-Sr-Ca-Cu-O superconductors*, Solid State Communications **71**, 819 (1989)

[29] P. Mandal, A. Poddar, B. Ghosh, and P. Choudhury, *Variation of* T_c *and transport properties with carrier concentration in Y- and Pb-doped Bi-based superconductors*, Phys Rev B **43**, 13102 (1991)

[30] K. Nanda Kishore, S. Satyavathi, V. Hari Babu and O. Pena, *Superconducting and normal state properties of the* $Bi_{1.7}Pb_{0.3}Sr_2Ca_{2-x}Y_xCu_3O_y$ *system*, Materials Science and Engineering B **38**, 267 (1996)

[31] K. Nanda Kishore, S. Satyavathi, M. Muralidhar, O. Pena and V. Hari Babu, *Effect of* Y^{3+} *substitution for Ca on the superconducting and the normal state properties of Bi(2223) system (*$Bi_{1.7}Pb_{0.3}Ca_{2-x}Y_xSr_2Cu_3O_y$*)*, Physica C , **235-240**, 1521 (1994).

[32] T. Kanai, T. Kamo, and S. Matsuda, *Dopant Effects on the Superconductivity in the Bi-Sr-Ca-Cu-O System*, Japan. Journal of App. Phys. 28, L551-554 (1989)

[33] G. Ilonca, A. V. Pop, T. R. Yang, I. G. Deac, C. Lung, R. Stiufiuc, and G.Stiufiuc, *Effects of rare earth ion substitution for Ca in (Bi,Pb):2223 superconductors*, International Journal of Inorganic Materials **3,** 769–772 (2001).

[34] P. Sumana Prabhu, M. S. Ramachandra Rao, U. V. Varadaraju, and G. V. Subba Rao, *T_c suppression and conduction mechanisms in $Bi_{2.1}Sr_{1.93}Ca_{0.97-x}R_xCu_2O_{8+y}$ (R=Pr, Gd, and Er) systems*, Phys Rev B **50**, 6929 (1994).

[35] K. Nanda Kishore, S. Satyavathi, V. Hari Babu and O. Pena, *Transport and magnetic properties of Sm-substituted BISCCO (2223) superconductors ($Bi_{1.7}Pb_{0.3}Sr_2Ca_{2-x}Sm_xCu_3O_y$)*, Physica C, **235**, 1519 (1994).

[36] O. Ozturk, M. Akdogan, H. Aydin, M. Yilmazlar, C. Terzioglu, and I. Belenli, *Substitution of Sm at Ca site in $Bi_{1.6}Pb_{0.4}Sr_2Ca_{2-x}Sm_xCu_3O_y$ superconductors*, Physica B **399,** 94–100 (2007)

[37] C. Terzioglu, M. Yilmazlar, O. Ozturk, and E. Yanmaz, *Structural and physical properties of Sm-doped $Bi_{1.6}Pb_{0.4}Sr_2Ca_{2-x}Sm_xCu_3O_y$ superconductors*, Physica C **423**, 119 (2005).

[38] M. Yilmazlar, H. A. Cetinkara, M. Nursoy, O. Ozturk, and C. Terzioglu, *Thermal expansion and Vickers hardness measurements on $Bi_{1.6}Pb_{0.4}Sr_2Ca_{2-x}Sm_xCu_3O_y$ superconductors* , Physica C **442,** 101 (2006).

[39] D. Yegen, A. Varilci, M. Yılmazlar, C. Terzioglu, and I. Belenli, *Magnetic properties of Sm-doped Bi-2223 superconductor studied by low field local Hall generator ac susceptibility*, Physica C , **466,** 5-10 (2007).

[40] K. Nanda Kishore, S. Satyavathi, M. Muralidhar, V. Hari Babu, O. Pena, M.Sergent, and F. Beniere, Physica Status Solidi (a), **143**, 101 (1994).

[41] K. Nanda Kishore, M. Muralidhar, V. Hari Babu, O. Pena, M.Sergent, and F. Beniere, *Effect of rare-earth Sm^{3+} substitution on the superconducting properties of the $Bi_{1.7}Pb_{0.3}Sr_2Ca_{2-x}Sm_xCu_3O_y$ system*, Physica C **204**, 299 (1993).

[42] D. R. Mishra, *Gd-substituted Bi-2223 superconductor*, Indian Academy of Sciences Pramana J. of Physics **70**, 535 (2008).

[43] R. Singh, A. Gupta, S. K. Agarwal, D. P. Singh, and A. V. Narlikar, *Superconductivity in Pr-doped $Bi_2Ca_2Sr_2Cu_3O_y$*, Supercond. Sci. Technol. **11**, 311 (1998)

[44] D. R. Mishra, P. L. Upadhyay, and R. G. Sharma, *Superconductivity of Nb-substituted Bi-2223 superconductor*, Physica C **304**, 293 (1998).

[45] A. Ekicibil, A. Coşkun, B. Özçelik, K. Kıymaç, *The Effect of Gd Concentration on the Physical and Magnetic Properties of $Bi_{1.7}Pb_{0.3-x}Gd_xSr_2Ca_3Cu_4O_{12+y}$ Superconductors*, Journal of Low Temp. Phys. **140**, 112 (2005).

[46] M. Sangeetha, M. Nagabhushanam , V. Haribabu , F. Beniere , and O. Pena, *Metal–insulator transition in $Bi_{1.7}Pb_{0.3}Sr_2Ca_{1-x}Gd_xCu_2O_{8-d}$ solid solutions*, Materials Science and Engineering B **58**, 258–262 (1999).

[47] A. Biju, R. G. Abhilash Kumar, R. P. Aloysius, U. Syamaprasad, *Structural and superconducting properties of $Bi_{1.7}Pb_{0.4}Sr_{2-x}Gd_xCa_{1.1}Cu_{2.1}O_y$ system*, Physica C **449,** 109 (2006).

[48] Y. Gao, P. Pernambuco-Wise, J. E. Crow, J. O'Reilly, N. Spencer, H. Chen, and R. E. Salomon, *Superconducting and magnetic phase boundaries in $Bi_2Sr_2Ca_{1-x}M_xCu_2O_8$, with M=Y, Gd, and Pr*, Phys. Rev. B **45,** 7436 (1992).

[49] X. Zhao, X. F. Sun, L. Wang, Q. F. Zhou, W. B. Wu, X. G. Li, Physica C **336**, 131 (2000).

[50] A. Sedky, *On the influence of rare-earth substitution for Ca in Bi(Pb):2212 superconducting system*, Physica C **468**, 1041 (2008).

[51] Y. Koike, Y. Iwabuchi, S. Hosoya, N. Kobayashi, and T. Fukase, *Correlation between T_c and hole concentration in the cation-substituted $Bi_2Sr_2CaCu_2O_{8+\delta}$ system*, Physica C **159,** 105 (1989).

[52] K. Koyama, S. Kanno, and S. Noguchi, *Electrical, Magnetic and Superconducting Properties of the High-T_c Superconductor $Bi_2Sr_2Ca_{1-x}RE_xCu_2O_{8+\delta}$ (RE=Nd and Pr)*, Jpn. J. Appl. Phys. **28,** 1354 (1989).

[53] N. Ichinose, and K. Saito, *Grain orientation of the Bi-Sr-Ca-Cu-O system ceramics by hotforging and their superconducting properties*, Physica C **190**, 177 (1992).

[54] Y. L. Chen, and R. Stevens, *2223 Phase Formation in Bi(Pb)-Sr-Ca-Cu-O: II, The Role of Temperature-Reaction Mechanism*, J. Am. Ceram. Soc. **75,** 1150 (1992).

[55] Y. L. Chen, and R. Stevens, *2223 Phase Formation in Bi(Pb)-Sr-Ca-Cu-O: I, The Role of Chemical Composition*, J. Am. Ceram. Soc. **75**, 1142 (1992)

[56] D. Y. Jeong, M. H. Sohn, D. W. Ha, I. R. Han, K. S. Ryu, Y. C. Kim, and S. K. Han, *Dependence of superconducting properties and microstructure on heat treatment in Ag-sheathed Bi-Pb-Sr-Ca-Cu-O tapes*, Physica C **185**, 2487 (1991).

[57] Keithley Instruments Inc. 1998 Handbook on Low Level Measurements 5th edn

[58] B. Chevalier, B. Lepine, A. Le Lirzin, J. Darriet, J. Etourneau and J.M. Tarascon, *Superconducting Properties Of Substituted Oxides $Bi_2Sr_2(Ca_{1-X}Y_X)Cu_2O_{8+y}$* Mater.Sci. Eng. B **2,** 277 (1989).

[59] B. Jayaram, P. C. Lanchester, and M. T. Weller, *Superconductivity and localisation in the $Bi_2Sr_2Ca_{1-x}RE_xCu_2O_{8+d}$(RE = Nd, Sm, Gd and Dy) system*, Physica C **160,** 17 (1989).

[60] A. Coskun, A. Ekicibil, B. Ozcelik, and K. Kiymac, *Field dependence of magnetization and dM/dH for Sm- and Gd-doped $Bi_{1.7}Pb_{0.3}Sr_2Ca_{2-x}RE_xCu_3O_{10+y}$ compounds*, Chin. Phys. Lett. **21**, 2041 (2004).

[61] M. Karppinen, A. Fukuoka, J. Wang, S. Takano, M. Wakata, T. Ikemachi, and H. Yamauchi, *Valence studies on various superconducting bismuth and lead cuprates and related materials,* Physica C **208,** 130 (1988).

[62] S. Simon, G. Ilonca, I. Barbur, I. Ardelean, R. Redac, *EPR on Y-ceramics and Bi-vitroceramics doped with S state paramagnetic ions*, Physica C **162-164**, 1289 (1989).

[63] H. J. Bornemann, D. E. Morris, H. B. Liu, and P. K. Narwankar, *Dependence of the oxygen isotope effect upon hole density in* $Bi_2Sr_2Ca_{1-x}Y_xCu_2O_{8+\delta}$ *and* $Y_{1-x}Ca_xBa_2Cu_4O_8$, Physica C **191**, 211 (1992).

[64] C. Terzioglu, H. Aydin, O. Ozturk, E. Bekiroglu, and I. Belenli, *The influence of Gd addition on microstructure and transport properties of Bi-2223*, Physica B **403**, 3354 (2008).

[65] A. Biju, R. P. Aloysius and U. Syamaprasad, *Enhanced critical current density in Gd-added (Bi, Pb)-2212 bulk superconductor*, Supercond. Sci. Technol. **18,** 1454 (2005).

[66] B. D. Cullity, Element of X-ray Diffraction, Addition–Wesley, Reading, MA, 1978

[67] C. W. Chu, L. Gao, F. Chen, Z. J. Huang, R. L. Meng,, and Y. Y. Xue, *Superconductivity above 150 K in* $HgBa_2Ca_2Cu_3O_{8+\delta}$ *at high pressures*, Nature **365,** 323 (1993).

[68] S. A. Halim, S. A. Khawaldeh, S. B. Mohammed, *Superconducting properties of* $Bi_{2-x}Pb_xSr_2Ca_2Cu_3O_y$ *system derived via sol-gel and solid state routes*, H. Azhan, Materials Chemistry and Physics **61**, 251 (1999).

[69] K. Nanda Kishore, S. Satyavathi, M. Muralidher, O. Pena, and V. Hari Babu, *Thermoelectric power studies on the Sm substituted BPSCCO (2223) superconductors*, Physica C **252,** 49 (1995).

[70] H. W. Zandbergen, W. A. Groen, A. Smit, and G. Vantendeloo, *Structure and properties of (Bi, Pb)$_2$Sr$_2$(Ca, Y)Cu$_2$O$_{8+\delta}$* , Physica C **168**, 426 (1990).

[71] A. Leenders, M. Ullrich and H.C. Freyhardt, *Influence of thermal cycling on the mechanical properties of VGF melt-textured YBCO*, Physica C **279,** (1997) 173.

[72] C. Veerender, V.R. Dumke, M. Nagabhooshanam*, Hardness and elastic moduli of Bi2-xPbxCa2Sr2Cu3Oy superconductors,* Phys. Status Solidi (a) **144,** 199 (1994).

[73] F.A. McClintock, A.S. Argon, *Mechanical Behaviour of Materials*, Addison-Wesley, Reading, MA, (p. 455) 1996.

[74] D. Tabor, *The Hardness of Metals*, Clarendon, Oxford, 1951

[75] B. R. Lawn, and T. R. Wilshaw, *Indentation fracture: principles and applications*, J. Mater. Sci. **10,** 1049 (1975).

[76] B.Y. Farber, N.S. Sidorov, V.I. Kulakov, A. Y. Lunin, A.N. Izotov, G.A. Emel'chenko, V.S. Bobrov, L.S. Fomenko, V.D. Natsik, S.V. Lubenets, Superconductivity **4,** 2296 (1991).

[77] M. Muralidhar, K.N. Reddy, V.H. Babu, *Microhardness Studies on BiCaSrCuO (2122) Superconducting Single Crystals and Pellets* ,Phys. Status Solidi (a) **126,** 115 (1991).

[78] H.C. Ling and M.F. Yan, *Microhardness measurements on dopant modified superconducting YBa$_2$Cu$_3$O$_7$ ceramics,* J. Appl. Phys. **64**, 1307 (1988).

[79] S.M. Khalil, *Enhancement of superconducting and mechanical properties in BSCCO with Pb additions*, Journal of Physics and Chemistry of Solids **62,** 457 (2001).

[80] A. Murakami, K. Katagiri, K. Noto, K. Kasaba, Y. Sohoji, M. Muralidhar, N. Sakai and M. Murakami, *Tensile mechanical properties of (Nd,Eu,Gd)–Ba–Cu–O bulk superconductors at room and liquid nitrogen temperatures,* Physica C **378**, 794 (2002).

[81] O. Ozturk, T. Kucukomeroglu, A. Varilci, I. Belenli and C. Terzioglu, Supercon. Sci. Technol. (accepted).

[82] J. Gong, J. Wu, Z. Guan, *Analysis of the indentation size effect on the apparent hardness for ceramics*, Mater. Lett. **38**, 197 (1999).

[83] R. Tickoo, R.P. Tandon, K.K. Bamzai, P.N. Kotru, *Microindentation studies on samarium-modified lead titanate ceramics*, Mater. Chem. Phys. **80,** 446 (2003).

[84] F. Fröhlinch, P. Grau, and W. Grellmann, *Performance and analysis of recording microhardness tests***,** Phys. Status Solidi (a) **42,** 79 (1997).

[85] H. Li, R.C. Bradt, *The microhardness indentation load/size effect in rutile and cassiterite single crystals,* J. Mater. Sci. **28,** 917 (1993).

[86] C. Hays, E.G. Kendall, An analysis of Knoop microhardness, Metallography **6,** 275 (1973).

[87] J.B. Quinn, G.D. Quinn**,** *Indentation brittleness of ceramics: a fresh approach,* J. Mater. Sci. **32,** 4331 (1997).

[88] O. Uzun, U. Kolemen, S. Celebi, and N. Guclu, *Modulus and hardness evaluation of polycrystalline superconductors by dynamic microindentation technique*, J. Europ. Ceramic Soc. **25,** 969 (2005).

CURRICULUM VITAE

Murat ERDEM

Address:

Abant İzzet Baysal University

Department of Physics

14280 Bolu, Turkey

Phone: +90 374 2541000

Fax: +90 374 2534642

Email: erdem_m@ibu.edu.tr

Personal Details:

Gender: Male

Date of Birth: May 5th, 1974

Place of Birth: Rencklinghausen ,Germany

Education:

1996 Middle East Technical University, Department of Physics undergraduate program

2002 MSc degree in Physics at Abant İzzet Baysal University

MSc Thesis: Analytical And Numerical Treatment of Partial Differential Equations In Physics

2009 PhD in Physics at Abant Izzet Baysal University

Conferences, Workshops and Schools:

- III. National Semposium of High Temperature Superconductors, Bolu, Turkey, 2005

  Poster : Effect of Annealing Time on $YBa_2Cu_3O_{7-x}$

  (M.Erdem, Ö.Öztürk, C.Terzioğlu, İ.Belenli, N.Türetken

- American Physical Society 2008 March Meeting, New Orleans, Louisiana, USA

  March 10-14, 2008

  Talk: Investigation of Some Physical Properties of Gd added Bi-2223 Superconductors

  (Murat Erdem, Özgür Öztürk, Hüseyin Aydın, Mustafa Akdoğan, Cabir Terzioğlu Ahmet Varilci, İbrahim Belenli**)**

  Talk: Mechanical and superconducting properties of $Bi_{1.8}Pb_{0.35}Sr_{1.9}Ca_{2.1}Cu_3Gd_xO_y$ system

  (Mustafa Akdoğan, Özgür Öztürk, Hüseyin Aydın, **Murat Erdem**, Cabir Terzioğlu)

- American Physical Society 2007 March Meeting, Denver, Colorado, USA

  March 5-9, 2007

  Talk: Orientation and Grain Boundaries in Bulk Samples of Bi-2223 Phase

  (**Murat Erdem**, Özgür Öztürk, Cabir Terzioğlu, İbrahim Belenli)

- Winter School on Basic Principles, Theories and Technological Application Fields of Superconductivity

  Sealife Hotel, Antalya , Turkey, January 24- February 01, 2009

- International Conference on Superconductivity and Magnetism (ICSM 2008)

  25-29 August 2008, Side-Antalya, Turkey

  Poster: The effect of extreme rolling on the properties of commercial MgB_2 tapes

  (E. Yucel, **M. Erdem**, I. Belenli)

Projects

- Investigation of the Electro-Optical Behaviour of Lantanide doped $(Bi,Pb)_2Sr_2Ca_2Co_3O_{10+X}$ thin Films under Radiation with different Wavelength in the vicinity of Transition.

  A.İ.B.Ü Bilimsel Araştırma Projeleri Fonu (BAP). Project No: 2003.03.02.194. **Researcher**.

Working Experience:

1997-2009 Working as a Research Assistant at the Physics Department of Abant Izzet Baysal University.